Early magmatism and the formation of a ‘Daly Gap’

at Akaroa Shield Volcano, New Zealand

A thesis submitted in partial fulfilment

of the requirements for the Degree of

Master of Science

in the University of Canterbury

by Eva Hartung

University of Canterbury

2011

TABLE OF CONTENTS

ACKNOWLEDGEMENTS

First of all, I would like to thank my supervisors, Dr Ben Kennedy, Dr Chad Deering and Dr Rose Turnbull for their invaluable assistance and encouragement throughout the period of this study.

Special thanks also to Aleysha Trent, Jon Gane, Lauren Foote, Kirsty Herbert and Peter Joint for their field assistance and to Rob Spiers (thin section preparation), Stephen Brown (XRF spectrometry) and Scott Kuehner (EMPA) for their technical assistance.

In addition, I would like to thank my family, friends, colleagues and staff in the Department of Geological Sciences for a wonderful time in New Zealand. This thesis would not have been completed without the continual encouragement and support of all these people.

And last, I gratefully acknowledge the research assistance with related expenses from the Mason Trust Fund of the University of Canterbury.

ABSTRACT

The origin of compositional gaps in volcanic deposits remains controversial. In Akaroa Volcano (9.6 to 8.6 Ma), New Zealand, a dramatic compositional gap exists between basaltic and trachytic magmas. Previously, the formation of more evolved magmas has been ascribed to crustal melting. However, the interpretation of new major and trace element analysis from minerals and bulk-rocks coupled with the mechanics of crystal-liquid separation offers an alternative explanation that alleviates the thermal restrictions required for crustal melting models.

In a two-stage model, major and trace element trends can be reproduced by polybaric crystal fractionation from dry melts (less than 0.5 wt.% H_2O) at the QFM buffer. In the first stage, picritic basalts are separated from an olivine-pyroxene dominant mush near the crust-mantle boundary (9 to 10 kbar). Ascending magmas stagnated at mid-crustal levels (5 to 6 kbar) and fractionated an olivine-plagioclase assemblage to produce the alkali basalt-hawaiite trend. In the second stage, trachyte melt is extracted from a crystal mush of hawaiite to mugearite composition at mid-to-upper crustal levels (3 to 5 kbar) after the melt has crystallised 50 vol.%. The fractionated assemblage of plagioclase, olivine, clinopyroxene, magnetite, and apatite is left in a cumulate residue which corresponds to the mineral assemblage of sampled ultramafic enclaves. The results of trace element modelling of Rayleigh fractionation using this extraction window is in close agreement with the concentrations measured in trachyte (= liquid) and enclaves (= cumulate residue). The compositional gap observed in the bulk-rock data of eruptive products is not recorded in the feldspar data, which show a complete solid solution from basalt and co-magmatic enclaves to trachyte. Complexly zoned plagioclases further suggest episodical magma recharge events of hotter, more mafic magmas, which lead to vigorous convection and magma mixing.

In summary, these models indicate that the Daly Gap of Akaroa Volcano formed by punctuated melt extraction from a crystal mush at the brittle-ductile transition.

INTRODUCTION

The origin of compositional gaps in volcanic deposits has remained controversial since Daly's first observations at mid-ocean ridges (Daly 1925; Barth 1939; Chayes 1963, 1977; Harris 1963; MacDonald 1963; Baker 1968; Claque 1978; Thompson 1972; Brophy 1991; Bonnefoi et al. 1995; Ferla and Meli 2006; Bachmann and Bergantz 2008). Some workers have previously argued that the scarcity of intermediate rock compositions between basalt and trachyte, often referred to as a "Daly gap", is the result of sampling bias (Harris 1963; MacDonald 1963; Baker 1968). However, the gap persists despite continued sampling and investigation on a worldwide basis (Chayes 1977; Claque 1978). Consequently, the absence of erupted parental magmas in a continuous sequence of crystal fractionation has led geologists to suggest that melting of some intermediate crustal lithology or igneous forerunner by basalt, similar to that erupted at the surface, produces the more evolved magmas (e.g Chayes 1963). Recent numerical models, however, have shown that the amount of melt production is small in regions of thin crust and conclude that the generation of voluminous felsic magmas and compositional variety is thermally restricted (Petford and Gallager 2001; Dufek and Bergantz 2005 and references therein).

Alternative models for generating compositional gaps include punctuated melt extraction from a rheological trapped crystal mush (Brophy 1991; Bachmann and Bergantz 2004, 2008; Hildreth 2004, Eichelberger et al. 2006). As basalt intrudes the crust rapid in-situ crystallisation occurs along the floors and ceiling of the magma chamber due to a temperature gradient between the wall-rock and intruding magma body (Marsh 1981). Subsequent buoyancy-driven convection arises from compositional changes caused by fractional crystallisation processes (Rice 1981; Sparks et al. 1984). Temperature-driven convection may also take place from phase changes as crystallisation proceeds. At a critical crystallinity of about 50 to 55 vol.% the magma approaches a rheological locking point or Rigid Percolation Threshold (RPT) where chamber-wide convection ceases (Vigneresse et al. 1996). If the viscosity and buoyancy is suitable the melt may migrate

upwards from the rigid crystalline framework to form two magma bodies of different composition (crystal cumulate residue and liquid). Recent multiphase numerical models indicate that crystal-liquid segregation occurs rapidly and most effectively within a crystal window of 50 to 70 vol.% (Dufek and Bachmann 2010) as a consequence of limited convection, latent heat buffering and reduced thermal gradients at the chamber walls.

At Akaroa Volcano, New Zealand, a distinct compositional gap (50 to 60 wt.% SiO_2; Fig. 1) exists in both the eruptive and intrusive products between basalt and trachyte, and gabbro and syenite, respectively. The formation of more evolved magmas has been previously related to melting of old continental crust (Weaver and Smith 1989). The interpretation of new radiogenic and stable isotopes analyses, however, indicates that magmas are predominantly mantle derived with only a minor component of crustal assimilation during the magmatic evolution of Akaroa Volcano (Timm et al. 2009). This rules out an origin by pure partial melting of old continental crustal lithologies and is consistent with thermal models that predict low degrees of crustal melt production. Hence, questions remain as to 1) what are the dominant processes that define the transition from basaltic to trachytic volcanism, 2) what magmatic processes generate the bimodal distribution ('Daly Gap') of Akaroa lavas, and 3) what are the relationships between the shallow intrusive rocks and extrusive rocks of Akaroa Volcano.

In this study, I examine the petrological features and bulk-rock and mineral chemistry of both mafic and felsic extrusive and intrusive rocks to better understand the magmatic system of Akaroa Volcano. Furthermore, I combine this geochemistry with a physical model of crystal-liquid segregation to explain the bimodal character of the early shield-forming stage of Akaroa Volcano. The results of my study are consistent with a two-stage fractionation model that produces evolved magmas by melt extraction from a crystal mush at mid-crustal levels within an optimal extraction window of 50 to 80 vol.%.

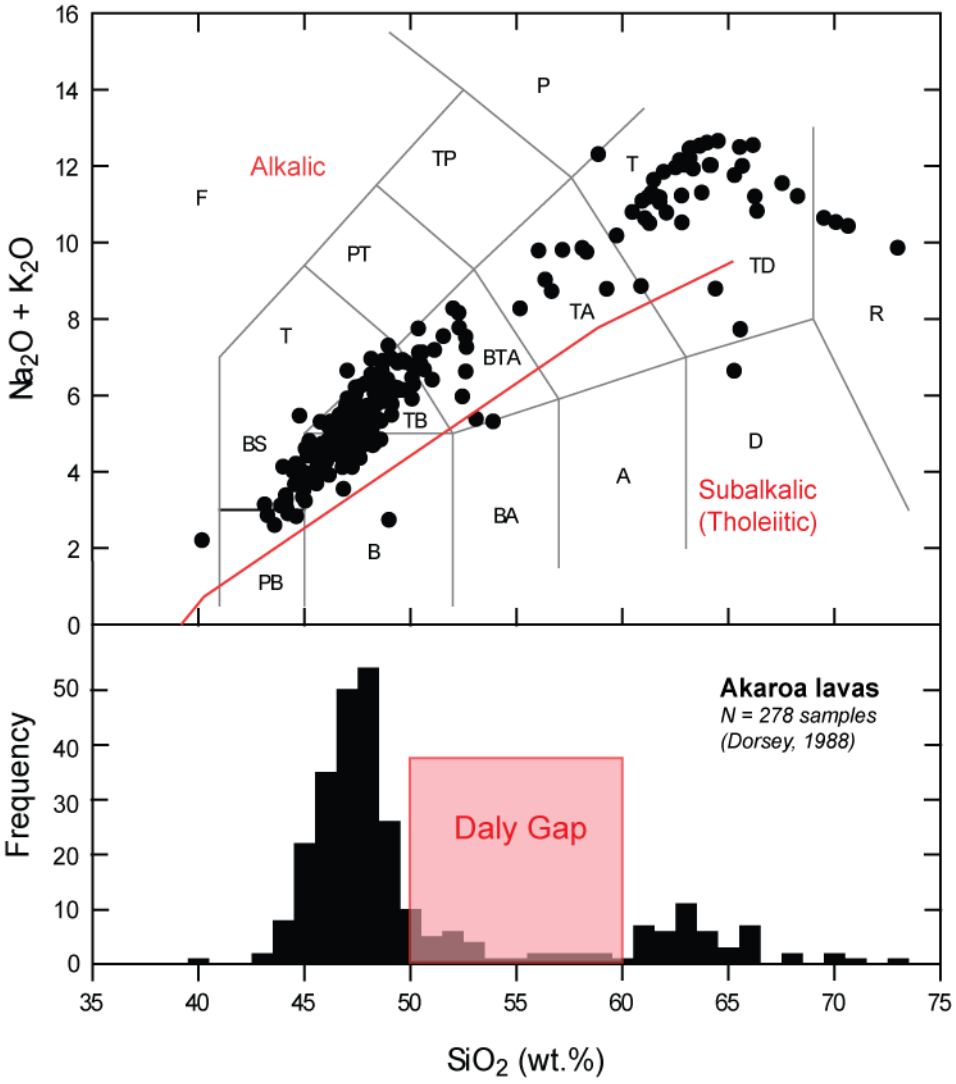

Fig. 1: Modal abundances of Akaroa rock compositions; Total alkalis vs. silica content are displayed in the upper figure. The frequency of Akaroa lava is displayed below. The near-absence of intermediate rock compositions between basalt and trachtyte is referred to as Daly Gap. Rock abbreviations: F – Fiodite, Bs – Basanite, T – Tephrite, PT – Phonoterphite, TP – Tephritic Phonolite, P – Phonolite, TB – Trachybasalt, BTA – Basaltic Trachybasalt, TA – Trachyandesite, TD – Trachydacite, T – Trachyte, PB – Picritic Basalt, B – Basalt, BA – Basaltic Andesite, A – Andesite, D – Dacite, R – Rhyolite (after Le Maitre et al. 2002).

GEOLOGICAL HISTORY

Continental intraplate volcanism was widespread in New Zealand throughout the Late Cretaceous and Cenozoic (Weaver and Smith 1989). Today, Banks Peninsula presents the most prominent volcanic landform on the South Island of New Zealand and comprises the eroded remnants of two large, dissected shield volcanoes (Lyttelton and Akaroa) and the contemporaneous Mt Herbert Volcanic Group (Fig. 2). Active during the Mid- to Late-Miocene (12.4 to 6.8 Ma; new $^{40}Ar/^{39}Ar$ ages from Timm et al. 2009), most lavas from Lyttelton Volcano and Akaroa Volcano formed rapidly within, approximately, one million years during two voluminous shield-building stage. Each shield stage was followed by a period of late-stage volcanism of one to two millions years (i.e. Mount Pleasant Formation, Diamond Harbour Volcanic Group). The coalescing volcanoes were built on Permian-Triassic Torlesse sediments (exposed at Lyttelton Volcano) and Late-Cretaceous volcanics of the Mount Somers Group. At first, Banks Peninsula formed an island which became connected to the mainland by extensive erosion of the Southern Alps mountain range and east-ward progradation in the Quarternary, about 20 000 years ago (Ligett and Gregg 1965).

Akaroa Volcano (9.4 to 6.8 Ma) represents the younger and larger construct of Banks Peninsula and is with an original diameter of about 50km (Weaver and Smith 1989) comparable in size to similar types of volcanoes globally (e.g. Mt Etna). The deposits of Akaroa Volcano were first described by Von Haast (1860) and have been studied by many workers since (Speights 1917, 1923, 1940, 1944; Ligett and Gregg 1965, Stipp and McDougall 1968, Price and Taylor 1980; Falloon 1982; Thiele 1983; Sewell 1985, 1988; Barley and Weaver 1988; Weaver and Sewell 1986, Dorsey 1988, Sewell et al. 1993; Johnston et al. 1997; Timm et al. 2009). The stratigraphic units of the whole of Akaroa Volcano are defined by seven formations (Sewell 1988) which include mafic and felsic volcanic products from central, flank and parasitic vent eruptions as well as shallow intrusions and minor plutonics (gabbro and syenite, exposed at Onawe Peninsula).

Hawaiian and mildly Strombolian style eruptions of basaltic to hawaiite lavas dominated the shield-forming stage of Akaroa Volcano and are similar to those described at Lyttleton volcano (Hampton et al. 2009). The early and late phases of the shield-building stage at Akaroa Volcano were accompanied by trachytic volcanism and include tuff rings, surge and block and ash flow deposits, and lava dome intrusions, respectively.

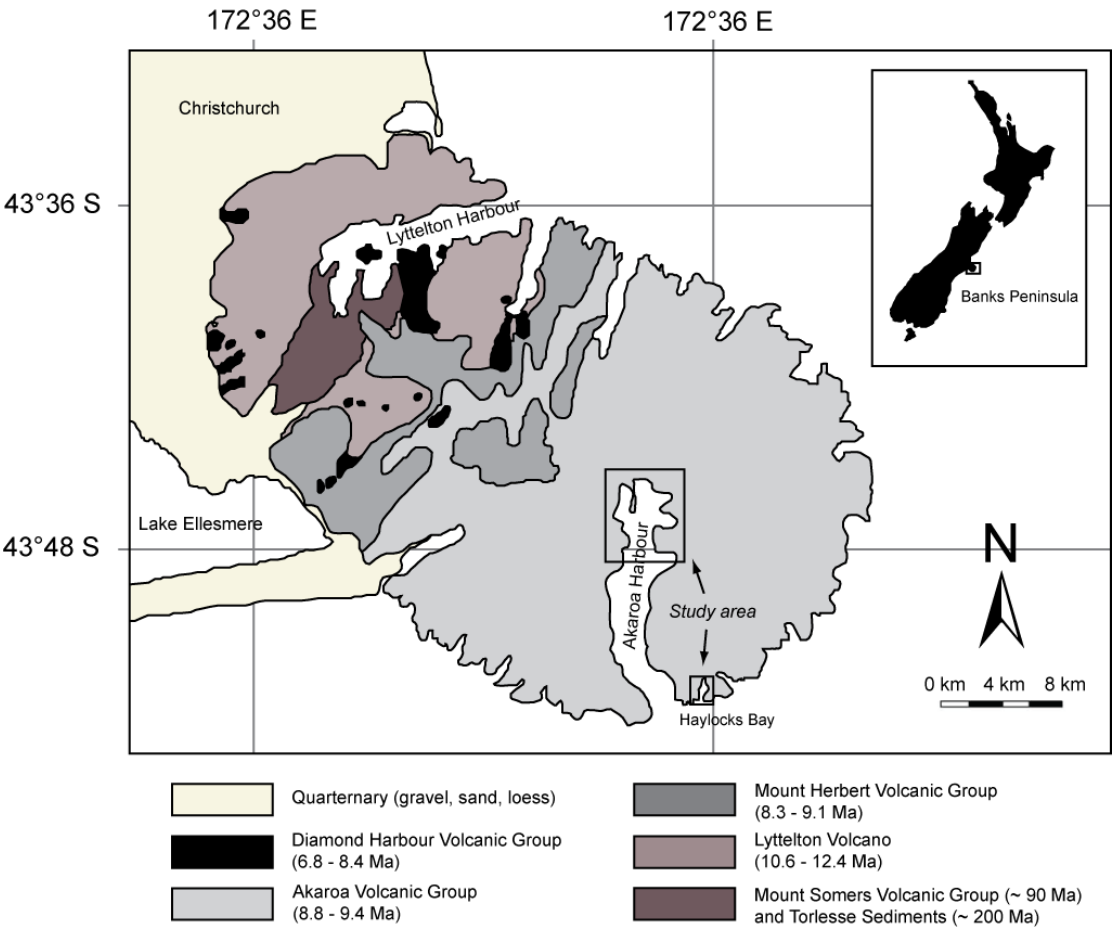

Fig. 2: Modified map of Banks Peninsula after Hampton and Cole (2009). New ages are from Timm et al. (2009). Study areas are indicated by black squares.

STRATIGRAPHY OF AKAROA HARBOUR

Volcanic deposits around the central harbour of Akaroa reflect the early emergent phases of volcanic activity above sea level at Akaroa Volcano (Fig. 3). Stratigraphic descriptions by Dorsey (1988) and Sewell (1988) and new field observations (also refer to Trent 2011, in prep.) indicate that the volcano underwent a transition from dominantly basaltic to trachytic volcanism and back to basaltic volcanism prior to Main Phase activity. An erosional unconformity indicates a period of dormancy and has been interpreted to mark the horizon between the Early and Main Phase of Akaroa Volcano (Dorsey 1988).

On the basis of previous work (Dorsey 1988, Sewell 1988) and our new field work (Trent 2011, in prep.) we propose the following stratigraphy for early stage volcanism of Akaroa Volcano from oldest to youngest: (1) Mafic and intermediate deposits of the Harbour Formation (defined in this study), (2) trachytic pyroclastics of the Lushington Breccia, (3) exogenous trachyte dome of the Tikao Trachyte, and (4) mafic lava flows and cinder cones of the younger French Hill Formation. Importantly, the French Hill Formation does not discriminate between the Early Phase and Main Phase deposits of the shield-building stage. Therefore we use the term early French Hill Formation in this chapter when referring to Early Phase deposits of Akaroa Volcano. At Haylocks Bay, the southern flanks of Akaroa Volcano (Fig. 2), co-magmatic enclaves are found within mafic lava flows of the French Hill Formation (Fig. 4), and could represent cumulate residues from early stage volcanism (Dorsey 1988).

Mafic lava flows and intermediate pyroclastics of the Harbour Formation *(ah)*, exposed on the west and east side of Onawe Peninsula, represent the oldest rocks of Akaroa Volcano (Dorsey 1988, Sewell 1988). Previously, these old deposits had been related to the French Hill Formation *(af)*, which describes most mafic volcanic deposits and late intrusive rocks that are associated with the main cone of Akaroa Volcano (Sewell 1988), including the deposits of the Early Phase.

However, because the mafic rocks on Onawe Peninsula clearly represent older units than trachyte deposits, we have allocated them to a new formation, the Harbour formation (also refer to Trent 2011, in prep.). On the west side of Onawe Peninsula the Harbour Formation defines a lava flow of alkali basalt, which is conformably overlain by a north-wards dipping welded, fine to coarse grained, polylithic lapilli tuff. This tuff comprises mugearite to benmoreite compositions and incorporates mudstone and sandstone clasts from the surrounding basement rocks (Dorsey 1988). On the east side of Onawe Peninsula alkali basalt to mugearite lava flows are overlain by a thin ash layer, which also forms part of the Harbour formation.

The Lushington Breccia *(al)* describes a sequence of at least four explosive trachytic events (pers. com. with Trent). Associated trachytic airfall deposits and pyroclastic surge deposits are exposed around Onawe and Takamatua Peninsula and north and south of French Farm Bay. The Lushington Breccia comprises interfingering facies of massive to poorly bedded, matrix to clast supported, poorly sorted trachyte breccia to lapilli tuff. Clasts are sub-angular to sub-rounded, typically up to 5 cm in size and often flow-banded or pumiceous. Boulder-sized clasts also occur occasionally. On the east side of Onawe Peninsula a fine trachytic lapilli tuff includes thin horizons of accretionary lapilli up to 5 mm in diameter indicating a period of phreatomagmatic eruptions (pers. com. with Trent). Explosive trachytic volcanism of Akaroa Volcano was accompanied by basaltic flank eruptions. Evidence for this is shown in the northwards dipping trachytic lapilli tuff on the eastern side of Onawe Peninsula, that contain impact sags from southwards dipping lava bombs (Fig. 4). Subsequent to this explosive stage an exogenous dome, which is mostly composed of pale to dark green, fine grained, aphyric to porphyritic trachyte (Tikao Trachyte, *at*), was emplaced between Petit Carenage Bay and Tikao Bay. The contacts to adjacent rocks are not exposed. However, trachytic dike intrusions incorporate clast lithologies of the Lushington breccia formation (Fig. 4), which indicates that the Tikao trachyte is younger than the Lushington breccia and not older as previously suggested (Sewell 1988). Within the dome structure trachyte rapidly

changes into a grey-white to purple-brown microsyenite that incorporates aggregates of coarse grained trachyte and syenite (Fig. 4).

After the emplacement of the Tikao Trachyte, volcanic activity changed entirely back to basaltic volcanism with monogenetic cinder cones and mafic lava flows centralised around the harbour. Olivine and plagioclase phyric alkali basalt and hawaiite are the dominant lava types and occur throughout the succession. Coarse grained and aphyric variations outcrop on the north-west and north-east side of Onawe Peninsula, respectively. Picritic basalts are present between Barrys Bay and French Farm Bay and on the east side of Onawe and Takamatua Peninsula. One lava flow with benmoreite composition exists on the east side of Onawe Peninsula and overlies the Lushington Breccia products. Ash deposits from cinder cones are typically characterized by red-brown, fine to medium ash that contains basaltic scoria and lava bombs.

The inner shorelines of Akaroa Harbour are extensively intruded by several cross-cutting radial dike swarms (0.1m to 6m width) of basaltic and trachytic composition, however trachytic compositions dominate. Onawe Peninsula dikes are entirely composed of trachyte and occur as large, up to 6m thick, dikes that radiate away from the central syenite intrusion. Only a few trachytic dikes cut the syenite, whereas the proximal volcanic deposits are almost entirely replaced by dike material.

The Duvauchelle Gabbro *(ad)* and Onawe Syenite *(ao)* are exposed on the southern tip of Onawe Peninsula, and represent younger plutonic equivalents to the volcanic rocks of the Akaroa Volcanic Group. Coarse-grained syenite forms a massive intrusion which weathers spheroidal and forms a convex upper surface, whereas the gabbro (Fig. 4) only appears as two small outcrops (5 to 10 m) northeast and northwest of the syenite. On the west side of Onawe Peninsula the contact between the gabbro and syenite is defined by a 1.2 meter thick trachyte dike. The contact on the east side is not observed. However, the difference in volume between both plutonic rocks, age dates (Timm et al. 2009) and field observations point to the syenite representing the younger intrusion. The relationship between the plutonic rocks and adjacent shallow dipping volcanic rocks

is poorly exposed. It has previously been considered to be intrusive as no major faults are mapped across the harbour (Dorsey 1988).

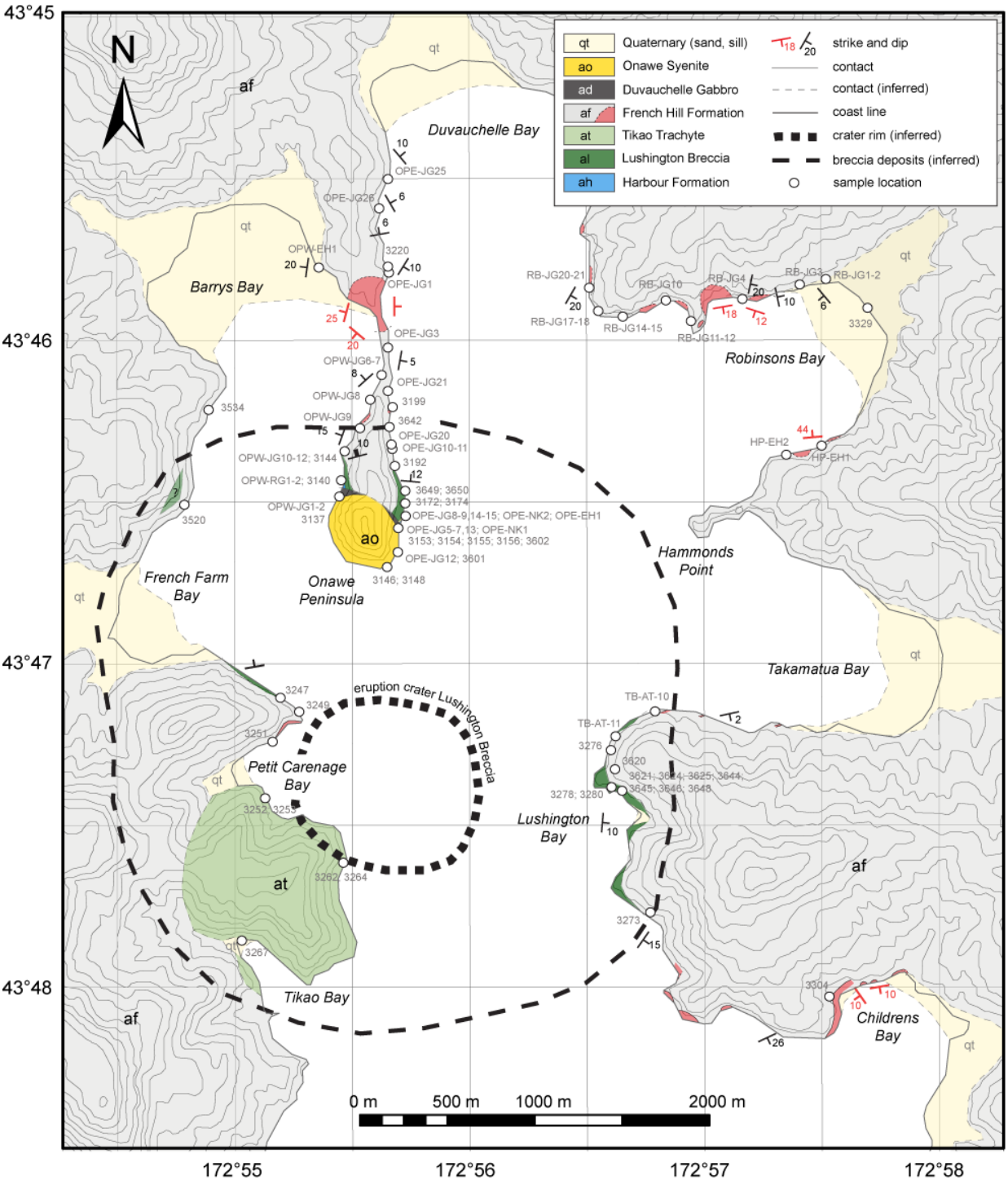

Fig. 3: Simplified geological map of the central part of Akaroa Volcano. The map represents a compilation of new field observations and interpretations (also refer to Trent 2011, in prep.) and previous geological maps created by Dorsey (1988) and Sewell (1988). Topographic contour lines are in intervals of 10 meters. Red areas and red strike and dip symbols refer to cinder cones and related ash deposits. Thin dashed lines represent inferred contacts between different deposits. Thick dashed black lines circle the eruption centre and outskirts of the Lushington Breccia deposits inferred from field measurements.

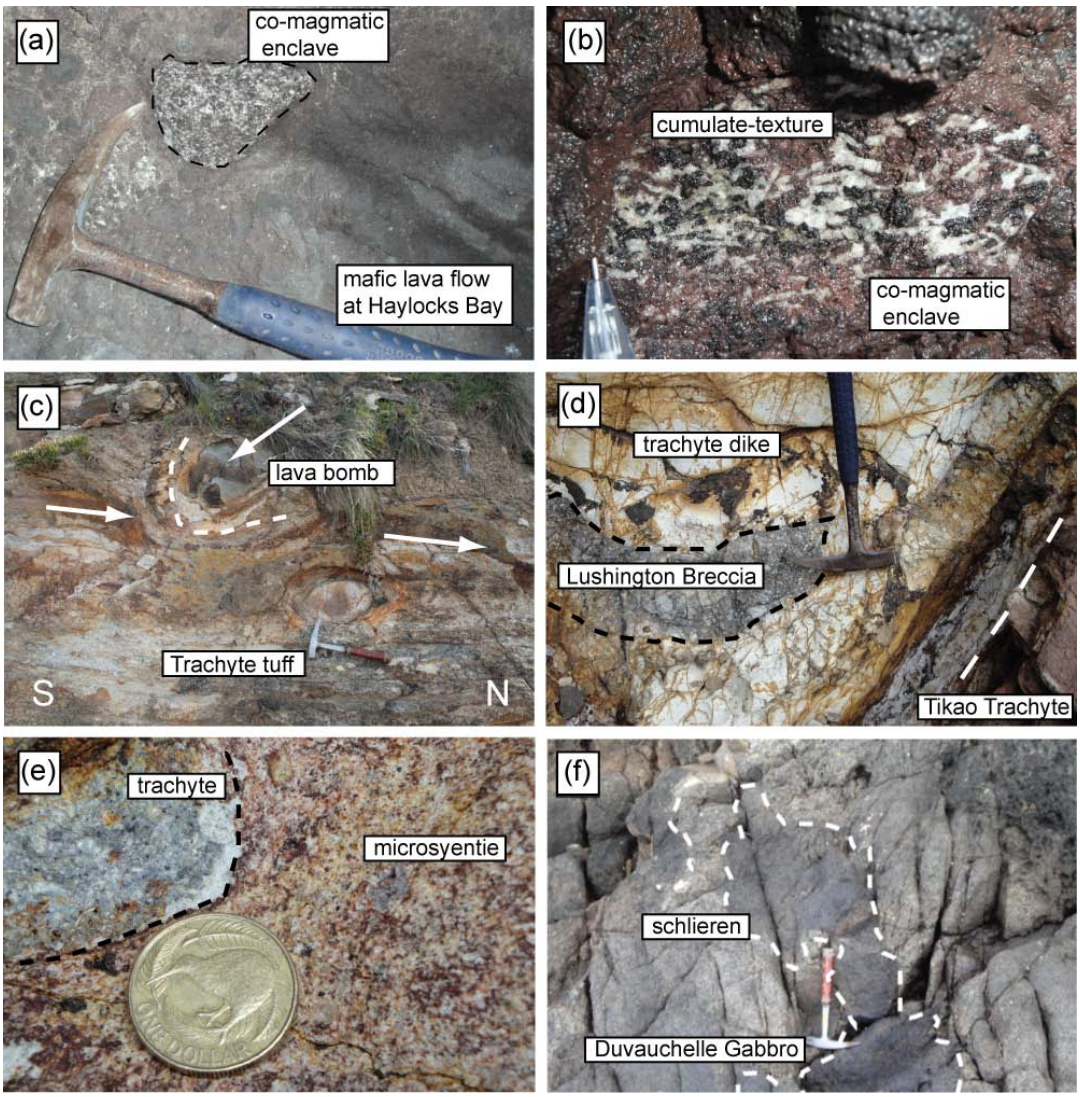

Fig. 4: Images of volcanic and plutonic products of Akaroa Volcano: (a) and (b) show co-magmatic enclaves in mafic lava flows of the French Hill Formation (af) at Haylocks Bay; (c) Trachytic lapilly tuff contains lava bombs from concurrent basaltic flank eruption; (d) A trachytic dike cuts the Tikao Trachyte (at) incorporating lithologies from the Lushington breccias (al); (e) Between Petit Carenage Bay and Tikao Bay grey-white microsyenite includes coarse grained aggregates of trachyte; (f) Felsic schlieren within the Duvauchelle Gabbro.

SAMPLING AND METHODS

This study builds on unpublished geochemical bulk-rock and mineral data from Dorsey's PhD thesis (1988). A detailed field investigation (about two month) was carried out along the inner shorelines of Akaroa Harbour with over 100 new samples collected from the volcanic and plutonic deposits (also refer to Trent 2011, in prep.). Co-magmatic enclaves were sampled from younger lava flows at Haylocks Bay (southern flank of Akaroa Volcano, see Fig. 2 for orientation) and separated from their host rocks. All rock samples were grouped according to rock composition, mineral assemblage and texture. Sixty seven rocks were examined in thin section of which fifteen selected and representative samples were studied petrologically in more detail. A large set of different mineral analyses were conducted including olivine, pyroxene, amphibole, biotite, feldspar and spinel. The modal composition of the rock was determined with an electromechanical point counter. Volume percentages were received by 800 counts and a stage interval of 2 for plutonic rocks and volcanic rocks.

XRF (X-ray fluorescence) analyses were conducted at the University of Canterbury, using a Philips PW 2400 Sequential Wavelength Dispersive X-ray Fluorescence Spectrometer calibrated to international standards (provided in supplementary data). The proportions of major elements were analysed by fused disc, and trace elements were analysed by pressed powder pellet. Glass fusion beads were prepared by fusing together approximately 1.3g of rock powder with 6.98g of flux ($Li_2B_4O_7$, Li_2O and La_2O_3 mixture) and a few grains of oxidant (NH_4NO_3) at 1030 ˚C for at least 15 minutes in Pt/Au crucibles. Loss on ignition (LOI) was calculated after fusion. Glass beads for major analysis were formed by pouring the molten material into Pt/Au moulds which are cooled rapidly. For trace element analysis approximately 8g of rock powder and polyvinyl alcohol solution (as a binder) were combined and pressed into 32mm diameter pellets in a hardened steel die at 3000 psi for 10 seconds. The major chemistry is determined on fusion beads using a rhodium

tube set at 50kV/55mA whereas the trace chemistry is determined on pressed powder pellets using a rhodium tube set at 60kV/46mA.

Major and trace element compositions of minerals were measured by electron microprobe analyses (EMPA) on a JEOL SUPERPROBE 733, equipped with four wave-length dispersed spectrometers, at the University of Washington. The machine was operating at an accelerating voltage of 15kV and a beam current of 15nA with a diameter of 1µm was used for olivine, pyroxene and spinel analyses. A defocused beam with a diameter of 3 µm was utilised for feldspar, amphibole and biotite analyses.

A total of 1170 new mineral analyses (reduced data) and 51 new bulk-rock analyses (reduced data) are presented in the following chapters. The complete data set is provided in the supplementary data, representative analyses are presented in Table 1 (bulk rock) and Tables 3 – 8 (mineral composition). To ensure a relative error of less than 1% only mineral analyses with anhydrous oxide totals of 100 ± 1 were retained for olivine, pyroxene and feldspar, 98 ± 1 for amphiboles and 96 ± 1 for biotite. Exceptions apply for high-resolution mineral profiles, which have a positive error of maximum 1 percent and negative error of maximum 2 percent. Furthermore, feldspar analyses of syenite are retained if totals are within 98.5 and 100 weight percent. For direct comparison of individual mineral analyses all mineral analyses were normalized to 100 % on an anhydrous basis. Bulk-rock chemistry was reduced to LOI percentages of less than 4 and normalized to 100 % for comparison. Despite, the high LOI value for syenite of 4.56, the sample analyses of OPE-JG12 have been retained as the sample appears less altered in hand sample and thin section compared to previously analysed specimens of syenite by Dorsey (1988). In general, all syenite speciments show some extent of alteration and need caution is recommended when making interpretations based on these analyses.

BULK-ROCK GEOCHEMISTRY

Representative whole-rock major and trace element analysis of volcanic rocks, plutonic rocks and co-magmatic mafic enclaves are recorded in Table 1 and plotted on selected Harker variation diagrams in Fig. 5 and Fig. 6. According to the TAS classification volcanic and plutonic products are of mildly alkaline character ('sodic' series, $Na_2O/K_2O > 2$) and range in composition from picritic basalt - alkali basalt – hawaiite – mugearite - benmoreite to trachyte and from gabbro to syenite, respectively. Co-magmatic enclaves are typically gabbroic in composition (38 to 48 wt. % SiO_2). A scarcity of intermediate rock compositions between 50 to 60 wt.% SiO_2 defines the 'Daly Gap' of the early phase of Akaroa Volcano.

Volcanic Rocks and shallow intrusives (*ah, al, at, af*)

Harker variation diagrams for major and trace elements show well-defined trends from mafic to felsic compositions. In general, concentrations of MgO, CaO, TiO_2, Cr, Ni, V and Sr progressively decrease with increasing SiO_2 content, where as concentrations of Na_2O, K_2O, Rb and Zr continuously increase with increasing SiO_2 content.

Mafic lavas (44 to 50 wt.% SiO_2) of the Harbour Formation and French Hill Formation include picritic basalt, alkali basalt and hawaiite with MgO contents ranging between 11 and 3.5 wt. %. Picritic basalts display distinctively higher MgO (< 10.4 wt.%), Ni (< 207 ppm) and Cr (< 418 ppm) contents than alkali basalts and hawaiites (Table 1).

Intermediate rock compositions (50 – 60 wt.% SiO_2) define mugearites and benmoreites from the Harbour Formation and French Hill Formation and contain less than 2 wt.% MgO. Lava flows of intermediate composition lie along the well defined trend from mafic to felsic rocks, however, tuff samples tend to plot away from the fractionation trend (i.e. Al_2O_3, Na_2O; Fig. 5).

Table 1: Representative major and trace element compositions of volcanic rocks, plutonic rocks and mafic enclaves

Rock type:	Picritic Basalt			Alkali Basalt			Hawaiite			Mugearite	Bemmoreite		
Details:	flow (glph)	flow (glph)	dike (glph)	flow (mg)	flow (fg)	flow (fg)	flow (aph)	flow (fg)	flow (fg)	flow (aph)	flow (aph)	sc. tuff	wd. tuff
Sample:	OPW-JG12	OPE-JG26	HP-EH2	OPW-EH1	OPW-JG7	RB-JG21	OPE-JG1	OPE-JG25	OPE-JG8	OPE-EH1	OPE-JG10	OPW-JG9	OPW-RG1
Formation	*af*	*af*	*af*	*af*	*af*	*af*	*af*	*af*	*ah*	*ah*	*af*	*af*	*af*
SiO_2	43.22	44.55	43.81	45.92	44.77	46.60	47.73	47.04	49.77	52.22	55.46	54.31	55.01
TiO_2	3.15	2.70	2.80	3.17	3.87	3.07	2.64	2.98	3.63	2.01	1.03	3.37	1.37
Al_2O_3	13.49	14.54	12.48	15.73	15.70	16.33	16.41	16.53	18.09	17.62	17.97	17.32	24.53
$Fe_2O_3^T$	13.80	13.24	13.70	13.70	13.79	13.05	13.19	12.96	13.20	12.31	9.01	12.84	11.79
MnO	0.17	0.17	0.17	0.17	0.17	0.18	0.21	0.20	0.22	0.25	0.18	0.09	0.05
MgO	9.39	7.53	10.38	5.86	5.37	5.32	3.80	4.46	1.75	1.80	1.34	0.48	0.86
CaO	10.91	11.06	10.77	9.32	9.81	8.31	7.09	7.59	6.32	3.98	2.75	2.85	0.86
Na_2O	2.02	2.67	2.94	3.32	3.30	3.70	4.91	4.30	4.03	5.17	5.94	4.00	2.54
K_2O	0.72	0.75	0.79	1.02	1.03	1.48	1.60	1.51	1.60	2.17	3.14	0.91	2.08
P_2O_5	0.29	0.41	0.37	0.38	0.66	0.79	1.12	1.01	0.73	0.80	0.58	0.83	<0.01
LOI	2.57	2.29	1.12	1.33	1.05	1.10	1.17	1.30	-0.19	0.94	2.52	2.91	0.85
Total	99.71	99.91	99.33	99.91	99.49	99.93	99.87	99.87	99.13	99.26	99.93	99.92	99.93
V	426	441	318	367	460	267	161	287	314	73	45	322	168
Cr	339	270	418	38	-	75	-	-	3	-	-	-	63
Ni	168	121	207	50	47	39	-	13	12	-	-	10	13
Zn	101	109	112	115	113	123	137	129	116	140	146	101	186
Ga	19	20	19	23	22	23	23	23	24	26	27	22	36
Rb	11	13	13	16	18	34	27	30	35	37	84	18	106
Sr	649	478	480	554	790	722	883	828	882	631	583	622	225
Y	21	24	25	30	27	33	45	38	39	49	50	29	60
Zr	136	145	177	187	210	292	299	278	287	423	535	237	624
Nb	39	39	45	47	57	76	85	76	76	112	131	74	142
Ba	245	224	295	256	473	411	548	503	550	560	903	390	892
Pb	-	1	-	-	2	3	-	4	1	4	5	-	13
Th	-	2	2	3	3	4	3	3	4	8	12	3	17
La	12	21	10	34	43	56	70	43	63	72	83	44	87
Ce	28	39	47	38	48	69	89	79	65	111	128	56	164
Nd	15	22	37	39	31	46	73	41	45	72	71	44	96

(Continued)

Table 1: Continued

Rock type:	Trachyte						Syenite		Gabbro			Mafic enclaves		
Details:	dike (fg)	dike (fg)	sill (glph)	*dome*	*tuff*	*breccia*	cg	*cg*	cg	cg	cg	cg	cg	cg
Sample:	OPW-JG8	OPE-JG3	OPE-NK2	*3252*	*3172*	*3625*	OPE-JG12	*3146*	OPE-JG13	OPE-JG5	OPW-JG2	HB-RT3	HB-RT4	HB-RT7
Formation	*af*	*af*	*af*	*at*	*al*	*al*	*ao*	*ao*	*ad*	*ad*	*ad*	*af*	*af*	*af*
SiO_2	65.29	68.16	59.44	*61.79*	*71.27*	*68.10*	57.64	*66.68*	42.16	40.81	43.38	43.22	41.99	39.17
TiO_2	0.22	0.22	0.58	*0.48*	*0.30*	*0.52*	0.65	*0.95*	3.66	5.27	3.93	4.42	5.31	5.18
Al_2O_3	16.51	16.45	18.72	*17.24*	*15.23*	*16.57*	16.83	*19.71*	17.87	15.68	16.74	18.76	17.79	13.08
$Fe_2O_3^T$	5.65	1.53	6.26	*6.12*	*0.65*	*1.47*	7.61	*0.95*	15.14	16.05	14.32	12.54	13.14	19.66
MnO	0.20	-	0.17	*0.10*	*0.02*	*0.06*	0.34	*0.03*	0.15	0.18	0.17	0.13	0.13	0.17
MgO	0.13	0.14	0.78	*0.31*	*0.36*	*0.15*	0.45	*0.13*	5.35	5.39	4.67	4.48	4.98	7.24
CaO	0.16	0.36	2.11	*1.73*	*0.13*	*0.59*	1.75	*1.11*	10.21	11.20	10.57	11.87	12.27	12.82
Na_2O	5.75	6.42	6.02	*6.96*	*3.92*	*4.95*	6.76	*7.46*	2.85	2.60	2.99	2.75	2.43	1.85
K_2O	5.11	5.21	3.78	*4.83*	*5.68*	*5.45*	3.08	*3.39*	0.39	0.33	0.39	0.34	0.26	0.20
P_2O_5	0.18	-	0.02	*0.13*	*0.04*	*0.06*	0.29	*0.02*	0.25	0.23	0.41	0.16	0.09	0.04
LOI	0.71	1.30	2.01	*0.23*	*1.45*	*1.24*	4.52	*0.37*	1.84	2.18	2.12	1.06	1.53	0.31
Total	99.91	99.79	99.87	*99.92*	*99.05*	*99.16*	99.91	*100.80*	99.88	99.91	99.70	99.72	99.92	99.71
V	28	-	33	*11*	*21*	*13*	24	*5*	571	728	467	268	254	617
Cr	26	-	22	*18*	*20*	*17*	-	*18*	-	-	-	29	-	-
Ni	4	-	-	*3*	*1*	*2*	-	*2*	30	12	13	23	31	69
Zn	142	29	111	*122*	*8*	*19*	146	*27*	106	110	112	89	88	140
Ga	33	31	32	*29*	*30*	*27*	29	*32*	22	21	22	21	21	22
Rb	188	142	76	*112*	*141*	*121*	84	*81*	4	-	4	3	-	-
Sr	15	13	335	*194*	*110*	*80*	227	*274*	559	522	580	891	823	564
Y	79	71	58	*57*	*44*	*33*	58	*43*	15	15	18	13	11	15
Zr	1008	623	673	*570*	*383*	*459*	498	*502*	78	80	93	78	84	71
Nb	196	170	180	*119*	*93*	*102*	114	*113*	22	29	31	19	24	15
Ba	281	27	865	*1481*	*366*	*1642*	865	*745*	210	353	232	151	125	116
Pb	19	11	7	*13*	*11*	*9*	7	*8*	-	-	2	-	-	-
Th	26	27	14	*13*	*19*	*14*	11	*9*	1	-	-	-	2	-
La	112	109	62	*86*	*66*	*54*	71	*65*	9	12	16	-	-	-
Ce	205	195	124	*156*	*169*	*107*	92	*102*	-	-	6	13	-	-
Nd	94	135	70	*70*	*68*	*37*	65	*56*	21	21	35	36	21	22

Abbreviations: glph - glomerophyric, cg – coarse grained, mg - medium grained, fg -fine grained, aph - aphanitic, sc. - scoriaceous, wd. – welded, LOI - loss of ignition; Major oxides are given in wt.% and trace element concentrations in ppm. Italic numbers represent analyses from Dorsey (1988).

Felsic lavas and pyroclastics from the Tikao Trachyte and Lushington Breccia, and younger dike intrusions (60 to 73 wt.% SiO_2) describe trachytes and rhyolitic trachtyes with MgO contents below 1 wt.%. The Lushington breccia and younger trachyte dikes exhibit more evolved compositions than the Tikao Trachyte (Table 1), which is characterized by lower silica contents of 61 to 62 wt.%. Overall, with the exception of K_2O and Rb, all major and trace elements are compatible and display decreasing trends with increasing silica abundance. Zircon, on the other hand, indicates two distinct trends: (1) An incompatible trend with increasing Zr concentrations (> 914 ppm) and (2) a compatible trend with decreasing Zr concentrations (< 673 ppm). In general, compositional trends of felsic rocks are not as well-defined as trends of mafic lavas.

Plutonic Rocks *(ad, ao)*

The Duvauchelle Gabbro (42 to 45 wt.% SiO_2) and Onawe Syenite (60 to 66 wt. SiO_2) form the two plutonic end-members of Akaroa Volcano. Intermediate compositions are either absent or not exposed.

Despite similar silica contents, the amount of major and trace elements differs quite substantially between the gabbro and picritic basalt. MgO contents of gabbro (6.4 to 4.6 wt.%) plot below the MgO abundances of picritic basalt. Simultaneously, gabbro composes much lower (< 23 ppm) Cr contents than picritic basalt. In comparison, MgO contents of alkali basalt are similar to contents in gabbro, however alkali basalt is more enriched in Cr than gabbro. TiO_2, Al_2O_3 and Na_2O contents in gabbro are enriched with respect to picritic basalt, but depleted in K_2O, Rb, Zr and Ni (< 36 ppm). CaO is enriched in gabbro with respect to alkali basalt and hawaiite, but depleted in Na_2O. Highest concentrations of V (377 – 728 ppm) are present in gabbro. Felsic schlieren and cavities within the gabbro represent compositions of monzodiorite and monozonite and show similar trends to their volcanic equivalents. However, concentrations of Rb and Zr are depleted with respect to volcanic rocks and syenite.

Syenite shows similar compositional trends as its volcanic equivalent trachyte and is characterized by low MgO, CaO, TiO_2, Ni, Cr, Sr and V and high Al_2O_3, Na_2O, K_2O, Rb and Zr with respect to mafic rocks. Yet, syenite displays a slightly higher sodium and lower potassium trend than trachyte.

Co-magmatic Enclaves (*af*)

Chemical compositions of co-magmatic enclaves are presented in Table 2. Major and trace element trends of co-magmatic enclaves differ distinctively from volcanic rock samples, but show similarities to the Duvauchelle Gabbro. Overall, mafic enclaves are enriched in TiO_2 (> 6 wt. %), CaO, Al_2O_3 and Sr and depleted in MgO, Na_2O, K_2O, Rb, Zr, V, Ni and Cr with respect to volcanic rock compositions.

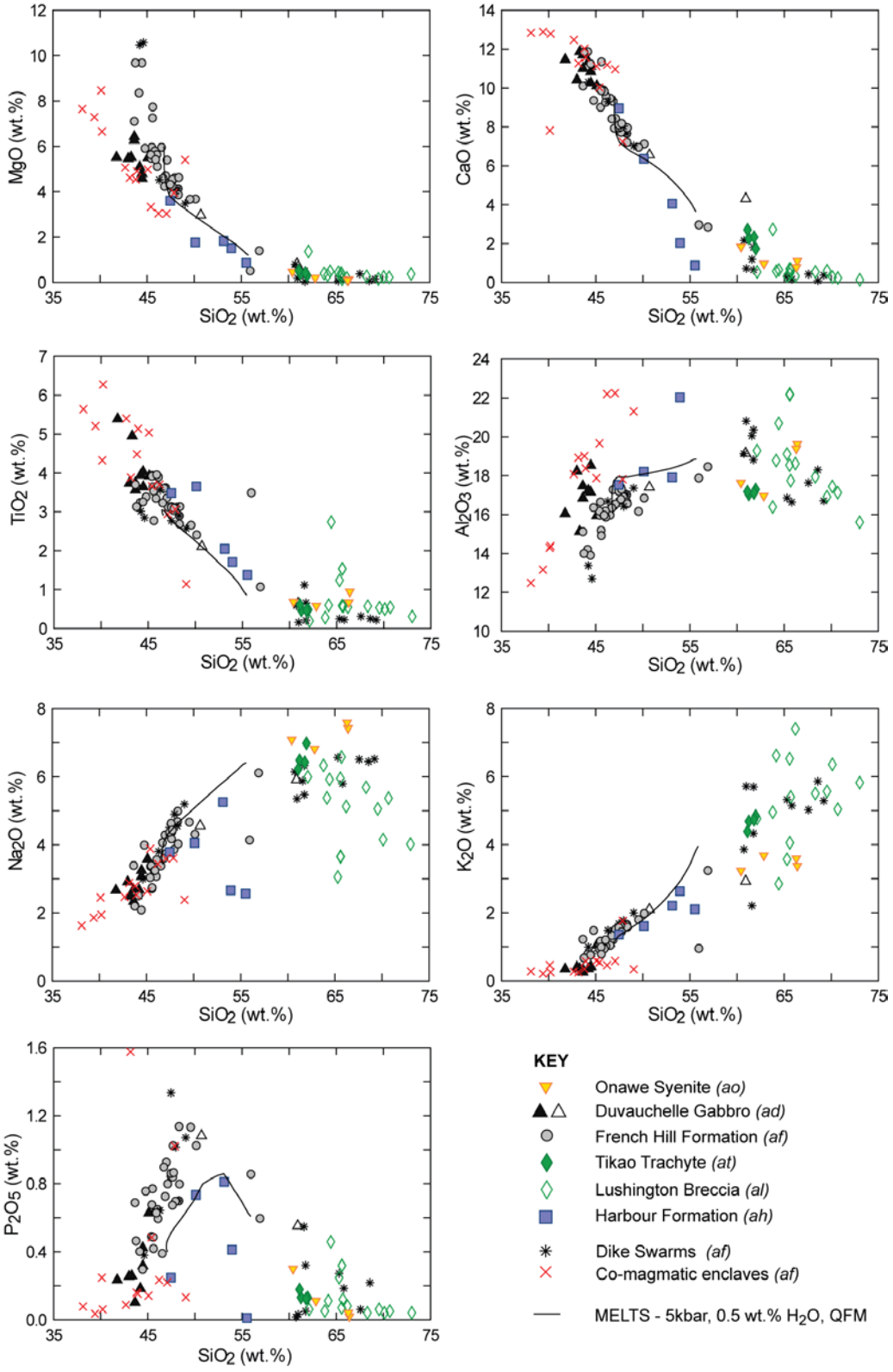

Fig. 5: Whole-rock major variation diagrams for the volcanic rocks, plutonic rocks and mafic enclaves of Akaroa Volcano.

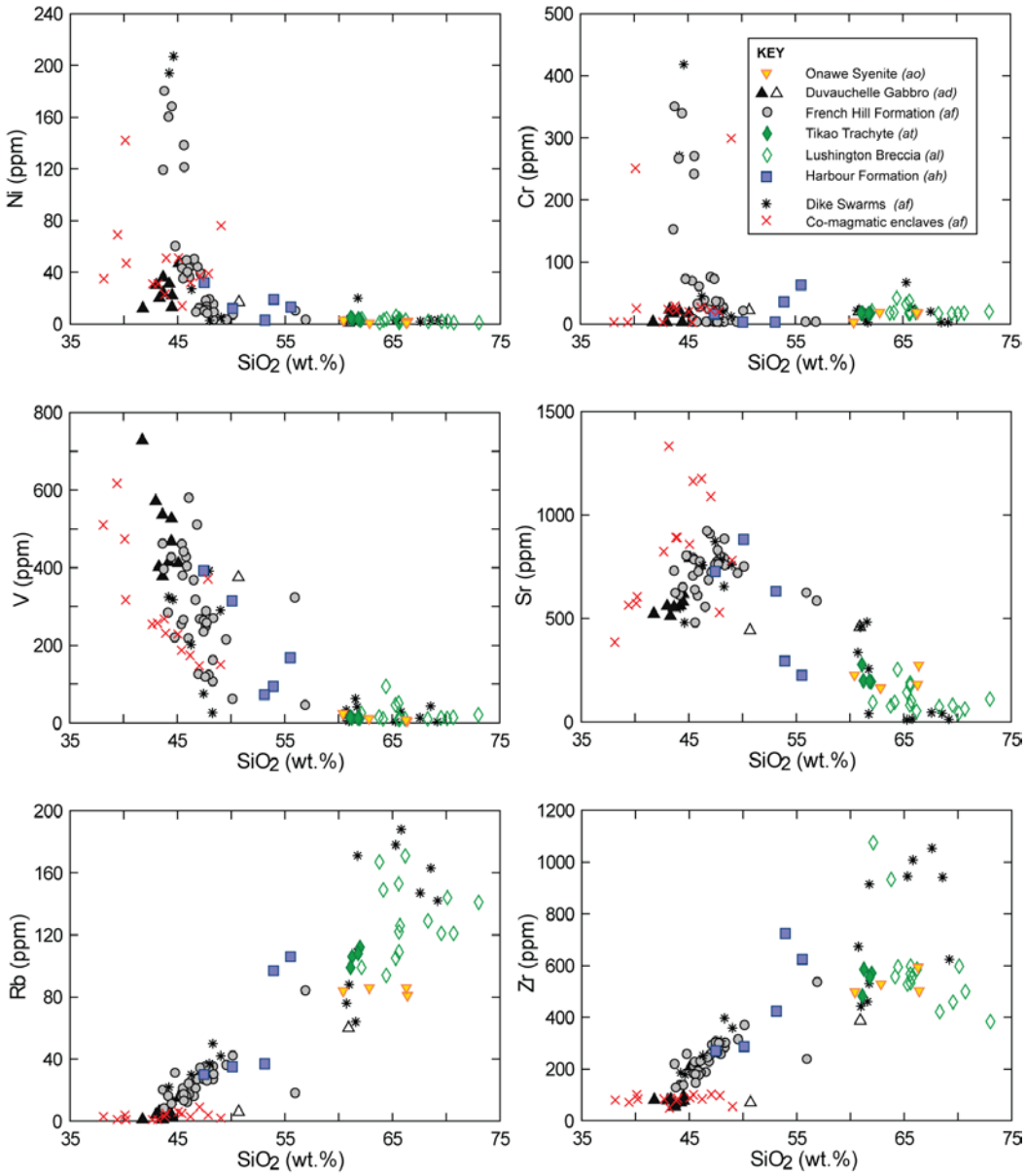

Fig. 6: Trace element variation diagrams for the volcanic rocks, plutonic rocks and mafic enclaves of Akaroa Volcano.

PETROGRAPHY

This chapter presents detailed rock descriptions of volcanic rock, plutonic rocks and co-magmatic enclaves. Detailed descriptions of pyroclastic units are presented by Trent (2011, in prep.) and Dorsey (1988).

Volcanic rocks

Picritic basalt (af)

Picritic basalt is porphyritic and seriate-textured (continuous range of crystal sizes). Phenocrysts and glomerocrysts of clinopyroxene and olivine (< 30%) are set in an intergranular, microcrystalline groundmass and range in grain size from 1mm up to 9mm (Fig. 7). Clinopyroxenes are typically euhedral to subhedral and display twinning, sector zoning, growth bands and marginal overgrowth along discrete dissolution surfaces. Some poikilophitic clinopyroxenes include equant olivine crystals and/or small laths of plagioclase (Fig. 8) and illustrate patchy zoning. Subhedral to euhedral olivine phenocrysts show pervasive breakdown reactions to iddingsite along concoidal fractures and throughout olivine microlites. Plagioclase microphenocrysts (< 1%) have spongy cellular cores with marginal overgrowths of clear plagioclase. The groundmass (< 0.1 mm) is composed of olivine, pyroxene, Fe-Ti oxides and aligned plagioclase lathes.

Olivine alkali basalt and hawaiite (ah, af)

Alkali basalt and hawaiite are typically porphyritic and seriate-textured and contain plagioclase and olivine phenocrysts (< 10%) that are embedded in a fine-grained, intergranular, holocrystalline groundmass. Complexly zoned plagioclase phenocrysts and microphenocrysts show a wide range of grain sizes up to 6mm with some having spongy cellular cores (Fig. 7). Olivine phenocrysts tend to be smaller (< 2mm) than plagioclase phenocrysts. Olivine

microphenocrysts are typically euhedral to subhedral and commonly pseudomorphed by calcite (Fig. 7). Occasional magnetite phenocrysts may be present (< 1%). Some basalts show an amygdoidal or vesicular texture, where amygdales (< 5 %) are commonly filled with finely crystallized calcite and/or zeolites. Microcrystalline lath-shaped feldspars are arranged subparallel in the groundmass, which additionally consists of clinopyroxene, olivine and spinel.

Coarse-grained alkali basalt (< 2mm) contains some multiple zoned plagioclase phenocrysts and displays intergranular and subophitic textures (Fig. 7) with interstitial oikocrysts of clinopyroxene enclosing plagioclase and olivine microcrystals. Aphanitic hawaiite may contain a few (< 1%) rounded crystals of brown apatite and clear plagioclase that are embedded in a cryptocrystalline groundmass (Fig. 7).

Mugearite and benmoreite (ah, af)

Mugearite and benmoreite lavas are typically aphanitic and aphyric. Occasionally, one or two complexly zoned plagioclase phenocrysts may be present (< 1%). Phenocrysts have resorbed cores which are overgrown by one or two discontinuous diffuse zones. Overall, plagioclase phenocrysts show disequilibrium texture (see Mineral Chemistry, Fig.14). The groundmass contains large amounts of Fe-Ti oxides, as well as clinopyroxene, olivine and feldspars.

Trachyte (al, at)

Trachytic lavas are typically holocrystalline, porphyritic or aphanitic. Feldspar-phyric lavas can reach phenocryst abundances of up to 30 vol.% with crystals up to 15mm in length. Some trachytes contain glomerophyric plagioclase phenocrysts and small amounts of biotite. Other samples contain green clinopyroxene phenocrysts (Fig. 8) and magnetite or green amphibole and trace amounts of fayalite (Fig. 7) in addition to alkali feldspar (Fig. 7). The groundmass is

generally composed of feldspar laths and minor amounts of iron oxides (< 2%). Additionally, clinopyroxene or hydrous minerals (i.e. biotite, amphibole) are present.

Table 2: Modal proportions of minerals from representative samples

Sample	*Rock type*	*Formation*	*Mineral abundance and percentages*
HB-RT2	enclave	*af*	Pl(37), Cpx (33), Ol(19), Fe-Ti oxide(11)
HB-RT3	enclave	*af*	Pl(60), Fe-Ti oxide(21), Cpx(19)
HB-RT4	enclave	*af*	Pl(59), Cpx(28), Fe-Ti oxide(10), Ol(3)
HB-RT7	enclave	*af*	Cpx(43), Pl (36), Sp(21)
OPW-JG2	gabbro	*ad*	Pl(56), Cpx(18), Fe-Ti oxide(16),Ol(4), Bt(3), Am(1), Kfs(1), Qtz(1), Ap(tr)
OPE-JG7	gabbro	*ad*	Pl(70), Cpx(12), Fe-Ti oxide(9), Ol(2), Bt(2), Am(1), Kfs(1), Qtz(1), Ap(2)
OPE-JG12	syenite	*ao*	Kfs(49), Pl(41), Fe-Ti oxide (5), Qtz(3), Fa(2), Zr(tr), Cz(tr)
OPW-JG12	picritic basalt	*af*	*Phc:* Ol(13), Cpx(6), Pl(tr) *Gm(81) :* Pl(42), Cpx(23), Fe-Ti oxide(12), Ol(4)
HP-EH2	picritic basalt	*af*	*Phc:* Cpx(17), Ol(13) Pl(tr) *Gm(70):* Pl(36), Fe-Ti oxide(20), Cpx(9),Ol(5)
OPW-EH1	alkali basalt	*af*	*Phc:* Pl(3) *Gm(97):* Pl(54), Cpx(26), Fe-Ti oxide(10), Ol(7)
OPW-JG6	hawaiite	*af*	*Phc:* Pl(5), Ol(4) *Gm(91):* Pl(43), Cpx(20), Fe-Ti oxide(23), Ol(5)
OPE-EH1	mugearite	*af*	*Phc:* Fs(tr) *Gm(100):* Fs(52), Cpx(23), Fe-Ti oxide(21),Ol(2), Ap(3)
OPE-NK2	trachyte (*sill)*	*af*	*Phc:* Fs(28), Bt(4) *Gm(68):* Fs(47), Bt(13), Fe-Ti oxide(8), Am(tr), Qtz(tr), Zr(tr)
3252	trachyte (*dome)*	*at*	*Phc:* Fs(5), Cpx(2) *Gm(93):* Fs(70), Cpx(14), Fe-Ti oxide(9), Zr(tr)
3148	trachyte (*dike)*	*af*	*Phc:* Fs(12), Am(2), Fa(tr) *Gm(86):* Pl, Am
OPE-JG3	trachyte (*dike)*	*af*	*Phc:* Kfs(tr) *Gm(100):* Kfs

Mineral abbreviations: Ol – Olivine, Cpx – Clinopyroxene, Pl – Plagioclase, Sp – Spinel Mineral Group, Am – Amphibole, Bt – Biotite, Qtz – Quartz, Kfs- Alkali feldspar, Ap – Apatite, Fa – Fayalite, Zr – Zircon, Cz – Clinozoisite, Fs – Feldspar, Phc – Phenocrysts, Gm – Groundmass,

Plutonic rocks

Gabbro (ad)

Coarse-grained gabbro has a phaneritic and equigranular texture (Fig. 7) and essentially consists of plagioclase, clinopyroxene, olivine, biotite, amphibole, iron oxides, some quartz (< 2 %) and accessory apatite. Modal abundances can vary significantly within the same unit (Table 2). Euhedral to subhedral plagioclase represent the dominant mineral phase. Crystals display multiple zoning of repeated discontinuous zones (see Mineral Chemistry, Fig. 14). Intergrowths and overgrowth of multiple and continuously zoned plagioclase, respectively, occur along discrete dissolution surfaces. Olivine is typically anhedral and fractures are often altered to red-brown iddingsite. Occasionally, crystals contain apatite inclusions (Fig. 8). Poikilitic clinopyroxene encloses a few equant olivine and plagioclase crystals. In more altered samples clinopyroxene and olivine are partly or completely pseudomorphed to calcite. Red-brown biotite and light-dark brown amphibole is typically subhedral. Amphibole shows alteration to allanite. Iron oxides and quartz are typically interstitial. Quartz occurs in trace amounts generally illustrating undulatory extinction. Apatite often occurs in clots as stubby grains of about 1mm, and is occasionally included in biotite (Fig. 7).

Some miarolitic cavities and felsic pockets in gabbro contain large (up to 2cm in size) crystals of plagioclase, alkali feldspar and quartz Feldspar crystals appear to be continuously zoned.

Syenite (ao)

Syenite is coarse-grained with a phaneritic, equigranular texture and mainly consists of microperthitic alkali feldspars and plagioclase and small proportions (< 10 %) of quartz, spinel and fayalite (Fig. 8). Biotite and amphibole have been reported in previous studies; however, biotite and amphibole were not found in samples from this study. Alkali feldspar often shows alteration to

sericite. Fayalite and clinopyroxene crystals are partly or completely replaced by calcite pseudomorphs. Voids are commonly infilled by quartz and some calcite. Micro-zircon, clinozoisite, and rutile are present in trace amounts.

Co-magmatic enclaves *(af)*

Ultramafic and mafic enclaves occur within the younger mafic lavas of the French Hill Formation (Fig. 4) and vary in size from a few centimeters to a couple of decimeters and in shape from subangular to subrounded. The grain boundaries between the host lava and co-magmatic enclaves appear abrupt and distinct (Fig. 8). All enclaves are holocrystalline, granular to intergranular and consist of plagioclase, clinopyroxene, olivine, and Fe-Ti oxides and show well developed igneous layering of thin, sub-parallel, discontinuous, monomineralic layers. Plagioclase and clinopyroxene represent the dominant mineral phases (>70 %). However, modal abundances of Fe-Ti oxide can make up to 21 vol.% of the rock (Table 2). Plagioclase is generally euhedral to subhedral, sometimes interstitial, and displays patchy zoning and complex resorption textures (Fig. 8). Elongated crystals may be aligned within granular clinopyroxene and olivine and intergranular Fe-Ti oxides. Olivine crystals are commonly replaced by red-brown iron oxides.

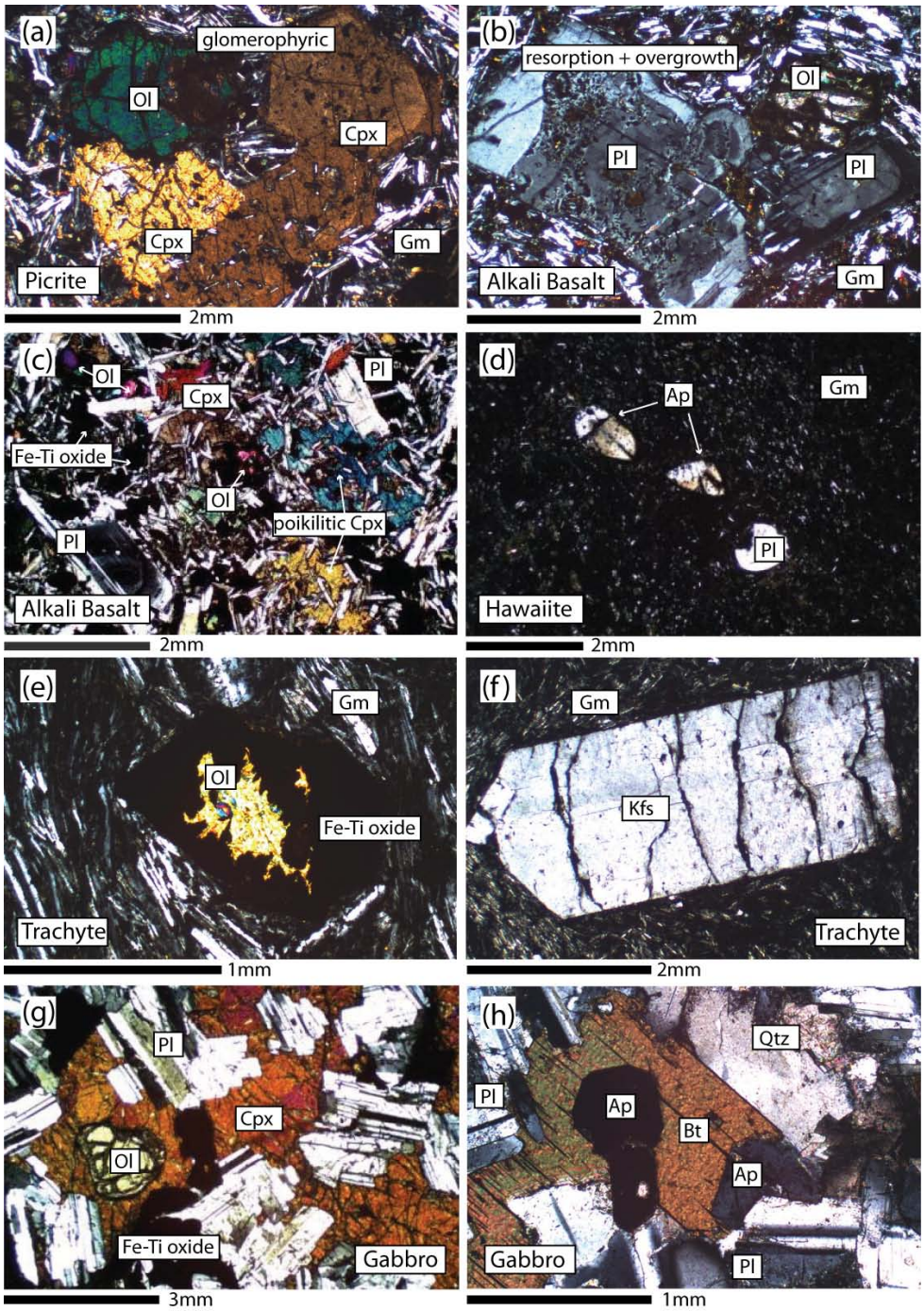

Fig. 7: Cross-polarised images of extrusive and intrusive lavas: (a) Porphyritic picritic basalt exhibits glomerophyric textures of olivine and zoned clinopyroxene phenocrysts. Poikilitic clinopyroxene encloses clear laths of plagioclase; (b) Alkali Basalt contains plagioclase and olivine phenocrysts. Resorbed plagioclase cores are overgrown with clear plagioclase. Subhedral olivine is pseudomorphed by calcite; (c) Coarse-grained alkali basalt with plagioclase, olivine, interstitial clinopyroxene and Fe-Ti oxides; (d) Aphanitic hawaiite contains occasional rounded apatite and plagioclase crystals; (e) Olivine phenocryst is surrounded by black Fe-Ti oxides in trachyte; (f) A single alkali feldspar phenocrysts is embedded in a fine-grained groundmass. (g) Gabbro is mainly composed by euhedral plagioclase, equant olivine, anhedral Fe-Ti oxide and interstitial clinopyroxene; (f) Accessory apatite is surrounded by biotite in quartz-bearing gabbro; Mineral abbreviations: Ol – Olivine, Cpx – Clinopyroxene, Pl – Plagioclase, Fe-Ti oxide – Iron-Titanium oxide, Bt – Biotite, Qtz – Quartz, Kfs- Alkali feldspar, Ap – Apatite, Gm – Groundmass.

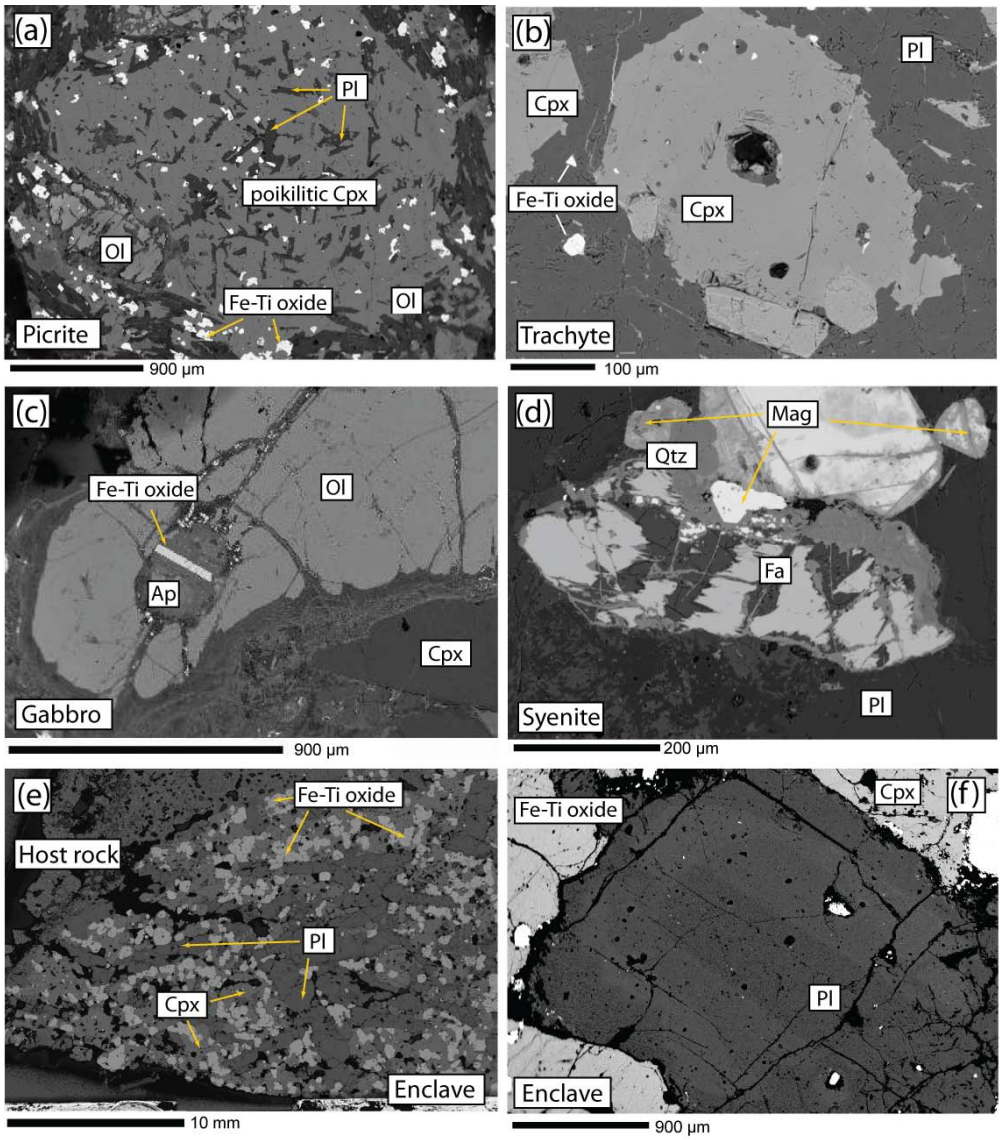

Fig. 8: Backscattered electron images of extrusive and intrusive lavas: (a) Patchy zoned poikilitic clinopyroxene includes olivine crystal, plagioclase lathes and Fe-Ti oxides; (b) Clinopyroxene phenocrysts in trachyte are embedded in a fine-grained groundmass of plagioclase and some Fe-Ti oxides; (c) Olivine in gabbro occasionally incorporates apatite crystals. In this picture Fe-Ti oxides forms a distinct surface within apatite; (d) Euhedral fayalite is adjacent to quartz and magnetite crystals and surrounded by plagioclase in syenite; (e) Co-magmatic enclave shows granular clinopyroxen, Fe-Ti oxide with interbedded and aligned elongated plagioclase crystals. The boundary between the host rock and enclave appears abrupt and distinct; (f) Zoned plagioclase crystal in co-magmatic enclave; Mineral abbreviations: Ap – Apatite, Ol – Olivine, Cpx – Clinopyroxene, Pl – Plagioclase, Fe-Ti oxide – Iron-Titanium oxide, Qtz – Quartz, Fa – Fayalite, Mag – Magnetite, Gm – Groundmass.

MINERAL CHEMISTRY

This chapter compares individual mineral compositions of volcanic and plutonic rocks, shallow magmatic intrusive (i.e. dike swarms) and co-magmatic enclaves.

Olivine

Representative chemical analyses of olivine in volcanic and plutonic rocks from Akaroa Volcano are recorded in Table 3 and compositional variation of olivine is illustrated in Fig. 9. Olivine data is consistent with previous analysis by Dorsey (1988). Phenocrysts are typically normally zoned and become progressively richer in iron towards the crystal rim. Olivine compositions vary moderately within each sample, but change overall from a forsterite-rich olivine in mafic volcanic rocks (picritic basalt, Fo_{81-66}; coarse-grained alkali basalt, $Fo_{78-41;}$ hawaiite, Fo_{65-58}) to a more fayalite-rich variation in mafic plutonic rocks (gabbro, Fo_{61-49}). Overall, groundmass olivine analyses are similar or more enriched in iron than phenocryst rim compositions (Fig. 10). Syenite contains few olivine crystals with fayalite contents of up to 96 % (Fo_{6-4}). Concentrations of Ni typically decrease with decreasing forsterite contents.

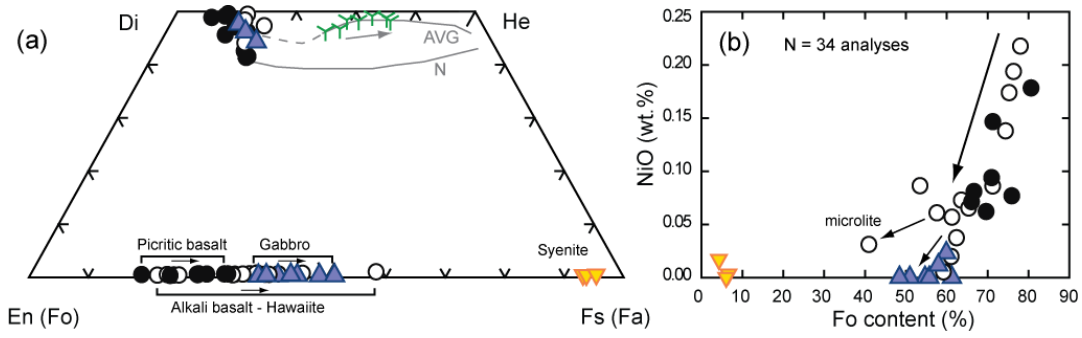

Fig. 9: Olivine compositions in volcanic and plutonic rocks from Akaroa Volcano. (a) Olivine and selected pyroxene analyses are plotted together in the pyroxene-olivine quadrilateral system En(Fo)-Fs(Fa)-Di-He. Pyroxene analyses of the Akaroa Volcanic Group (AVG) by Dorsey (1988) are shown for comparison. Olivine is typically normally zoned. (b) Variation diagram of NiO vs. forsterite content. NiO concentrations decrease with decreasing forsterite contents. Plutonic rocks display lowest NiO contents. Symbols are as in Figure 13.

Table 3: Representative analyses of olivine in volcanic and plutonic rocks

Rock type:	Picritic basalt			Alkali basalt			Hawaiite		Gabbro		Syenite
Sample:	*OPW-JG12*			*OPE-EH1*			*OPE-JG25*		*OPE-JG5*		*OPW-JG12*
Size:	*ph-c*	*ph-r*	*mc*	*ph-c*	*ph-r*	*mc*	*mph-c*	*mph-c*	*mph-c*	*mpc-r*	*mph-c*
SiO_2	38.27	36.66	36.98	38.44	36.98	33.60	36.54	36.98	35.20	34.80	29.94
Cr_2O_3	0.02	0.03	0.00	0.01	0.01	0.01	0.00	0.00	0.00	0.00	0.00
FeO	18.26	28.76	29.26	21.17	30.09	45.95	34.23	29.80	36.72	41.94	64.59
MnO	0.22	0.51	0.41	0.26	0.41	0.90	0.84	0.55	0.66	0.77	2.89
NiO	0.14	0.08	0.07	0.19	0.07	0.03	0.01	0.06	0.00	0.00	0.00
MgO	41.38	32.88	32.60	39.15	31.76	18.22	28.24	31.96	26.20	22.25	2.34
CaO	0.21	0.35	0.35	0.28	0.31	0.55	0.28	0.23	0.29	0.20	0.23
Total	98.50	99.26	99.67	99.50	99.62	99.27	100.14	99.59	99.08	99.97	99.99
Fo	*79.7*	*66.4*	*65.9*	*76.2*	*64.7*	*40.6*	*58.7*	*65.0*	*55.3*	*48.0*	*5.8*

Abbreviations: ph – phenocryst, mph – microphenocryst, mc – microlite, c – core, r – rim, Fo – forsterite; Oxides are listed in wt.%, Fo in mol %.

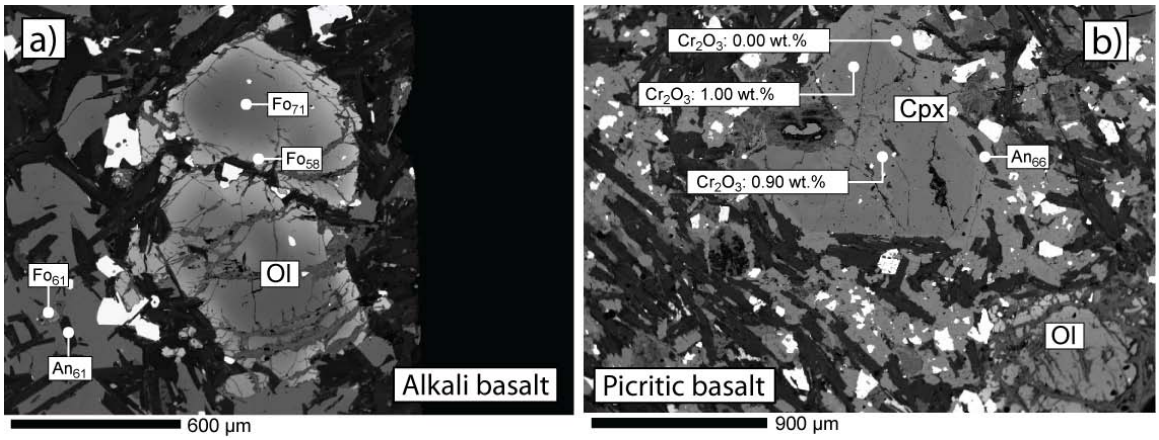

Fig. 10: (a) Normal zoned olivine phenocryst in alkali basalt. Interstitial pyroxene encloses olivine microlites with Fo_{61} and plagioclase laths with An_{61}. (b) A Cr-rich clinopyroxene phenocrysts encloses a small olivine crystal. Cr-poor pyroxene overgrowths contain plagioclase lathes with An_{66}.

Clinopyroxene

Representative pyroxene analyses are presented in Table 4. Stoichiometric calculations are corrected for Fe^{3+} based on four cations and six anions. Pyroxene compositions vary moderately between $Wo_{41-49}En_{40-44}Fs_{6-16}$ in picritic basalt, $Wo_{44-49}En_{37-42}Fs_{12-16}$ in alkali basalt and hawaiite, and $Wo_{46-49}En_{15-27}Fs_{27-37}$ in trachyte (Fig. 9, selected analyses). Most crystals are normally zoned from core to rim with some crystals being reversely zoned in trachytic lavas. In gabbro, analyses of pyroxenes reveal a fairly constant composition of $Wo_{44-47}En_{40-41}Fs_{13-16}$. Compositional trends from this study overlap with pyroxene data obtained by previous workers (Price and Taylor, 1980;

Dorsey, 1988). Variation of pyroxenes observed in similar Alkali Suites (Price and Chappell, 1975; Price and Taylor, 1980; Abbott, 1969), however, illustrate that pyroxenes of Akaroa Volcano are compositionally restricted to mainly diopside-hedenbergite with only a minor aegerine component (< 10 mol.%, Fig. 11). The change in whole-rock composition from pyroxene in mafic rocks to pyroxene in evolved rocks is defined by a sharp decrease of Al_2O_3 and TiO_2 (Fig.12) below diopside (Di) contents of ~ 57 %. In mafic lavas, Al_2O_3 and TiO_2 contents of clinopyroxene commonly increase towards the crystal rim, from 2.3 to 5.2 wt.% and 1.0 to 3.1 wt.%, respectively. Picritic basalt displays by far the highest Al_2O_3 contents of 3.1 – 8.2 wt.%. In trachyte, pyroxene concentrations of Al_2O_3 and TiO_2 are below 2.0 wt.% and 0.7 wt.%, respectively, and decrease with decreasing Di content. Cr_2O_3 concentrations are below 0.04 wt.% in trachytic rocks, below 0.1 wt.% in alkali basalt and hawaiite and generally below the detection limit (< 0.001 wt.%) in gabbro. However, phenocrysts in picritic basalt contain Cr_2O_3 concentrations of up 1 wt. % (Fig. 12). Furthermore, growth bands and marginal zoning in clinopyroxene are also associated with high Cr_2O_3 concentrations (< 0.8 wt. %, Fig. 12). However, poikilitic pyroxene that encloses plagioclase laths and pyroxene that overgrow normal zoned phenocrysts contain no Cr (Fig. 10).

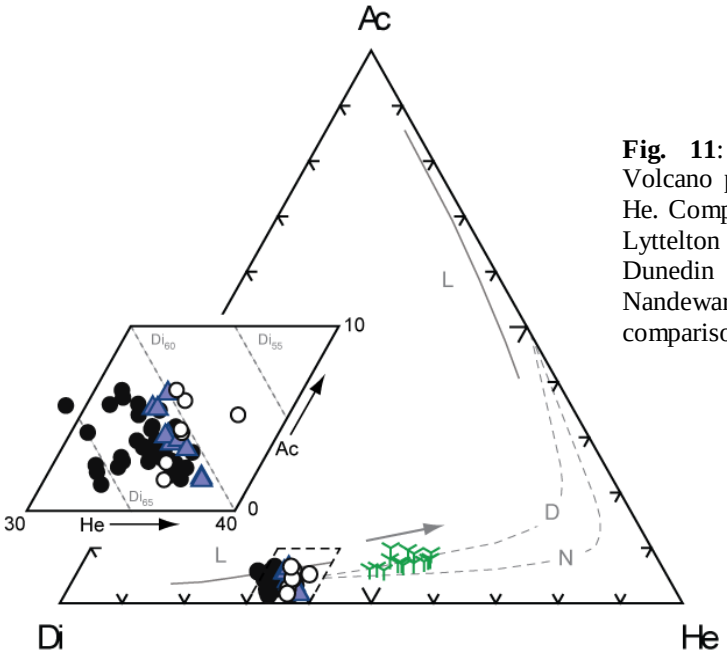

Fig. 11: Clinopyroxene analyses from Akaroa Volcano plotted in the quadrilateral system Ac-Di-He. Compositional variations of pyroxenes from L - Lyttelton Volcano (Price and Taylor, 1980), D – Dunedin (Price and Chappell, 1975) and N – Nandewar Volcano (Abbott, 1969) are shown for comparison. Symbols are as in Figure 13.

Table 4: Representative analyses of clinopyroxene in volcanic and plutonic rocks

Rock type:	Picritic basalt					Alkali basalt			Hawaiite	
Sample:	*OPW-JG12*					*OPW-EH1*			*OPE-JG25*	
Size:	*ph-c*	*ph-r*	*ph-c*	*ph-r*	*mc*	*in-c*	*in-r*	*in-r*	*mc*	*mc*
SiO_2	48.17	49.03	50.74	48.62	50.30	50.74	48.62	46.26	51.20	49.42
TiO_2	1.58	2.35	1.81	2.52	2.13	1.81	2.52	3.48	1.66	2.26
Al_2O_3	7.11	4.30	2.62	3.66	3.68	2.62	3.66	5.73	3.43	3.72
Cr_2O_3	0.90	0.00	0.03	0.01	0.02	0.03	0.01	0.08	0.00	0.00
FeO	5.91	7.81	8.86	11.03	8.09	8.86	11.03	9.20	8.85	9.56
MnO	0.08	0.14	0.16	0.23	0.16	0.16	0.23	0.14	0.26	0.27
NiO	0.04	0.00	0.00	0.03	0.00	0.00	0.03	0.02	0.00	0.00
MgO	14.22	13.69	14.09	11.84	13.47	14.09	11.84	12.03	13.18	12.84
CaO	21.55	21.44	20.76	21.17	21.17	20.76	21.17	21.50	21.04	21.52
Na_2O	0.49	0.46	0.37	0.57	0.54	0.37	0.57	0.53	0.83	0.69
Total	100.04	99.21	99.43	99.69	99.56	99.43	99.69	98.99	100.46	100.28
	$Wo_{49}En_{45}Fs_6$	$Wo_{47}En_{42}Fs_{11}$	$Wo_{44}En_{42}Fs_{14}$	$Wo_{47}En_{37}Fs_{16}$	$Wo_{46}En_{40}Fs_{14}$	$Wo_{44}En_{42}Fs_{16}$	$Wo_{47}En_{37}Fs_{16}$	$Wo_{49}En_{39}Fs_{12}$	$Wo_{46}En_{40}Fs_{14}$	$Wo_{48}En_{40}Fs_{12}$

(Continured)

Table 4: Continued

Rock type:	Trachyte				Gabbro		
Sample:	*3252*				*OPW-JG2*	*OPE-JG13*	*OPW-JG5*
Size:	*ph-c*	*ph-c*	*ph-r*	*mc*	*in*	*in*	*In*
SiO_2	50.06	49.77	50.50	49.36	51.43	48.77	48.30
TiO_2	0.66	0.60	0.38	0.25	1.03	2.12	2.38
Al_2O_3	2.00	1.79	0.58	0.82	2.26	4.41	4.35
Cr_2O_3	0.01	0.01	0.01	0.02	0.00	0.01	0.00
FeO	17.30	18.47	20.75	22.18	10.04	9.01	10.30
MnO	0.56	0.66	1.18	1.23	0.24	0.17	0.21
NiO	0.03	0.03	0.02	0.06	0.00	0.00	0.00
MgO	8.68	7.81	5.94	4.70	13.52	13.35	13.30
CaO	20.29	20.41	20.05	20.27	20.71	21.35	20.63
Na_2O	0.69	0.63	0.98	0.88	0.38	0.47	0.45
Total	100.30	100.19	100.39	99.78	99.6	99.66	99.92
	$Wo_{46}En_{27}Fs_{27}$	$Wo_{46}En_{25}Fs_{29}$	$Wo_{47}En_{19}Fs_{34}$	$Wo_{48}En_{16}Fs_{36}$	$Wo_{44}En_{40}Fs_{16}$	$Wo_{47}En_{41}Fs_{12}$	$Wo_{46}En_{41}Fs_{13}$

Abbreviations: ph – phenocryst, mph – microphenocryst, mc – microlite, c – core, r – rim, Wo – Wollastonite, En – Enstatite, Fs – Ferrosilite; Oxides are listed in wt.%., $Wo_{xx}En_{xx}Fs_{xx}$ in mol %.

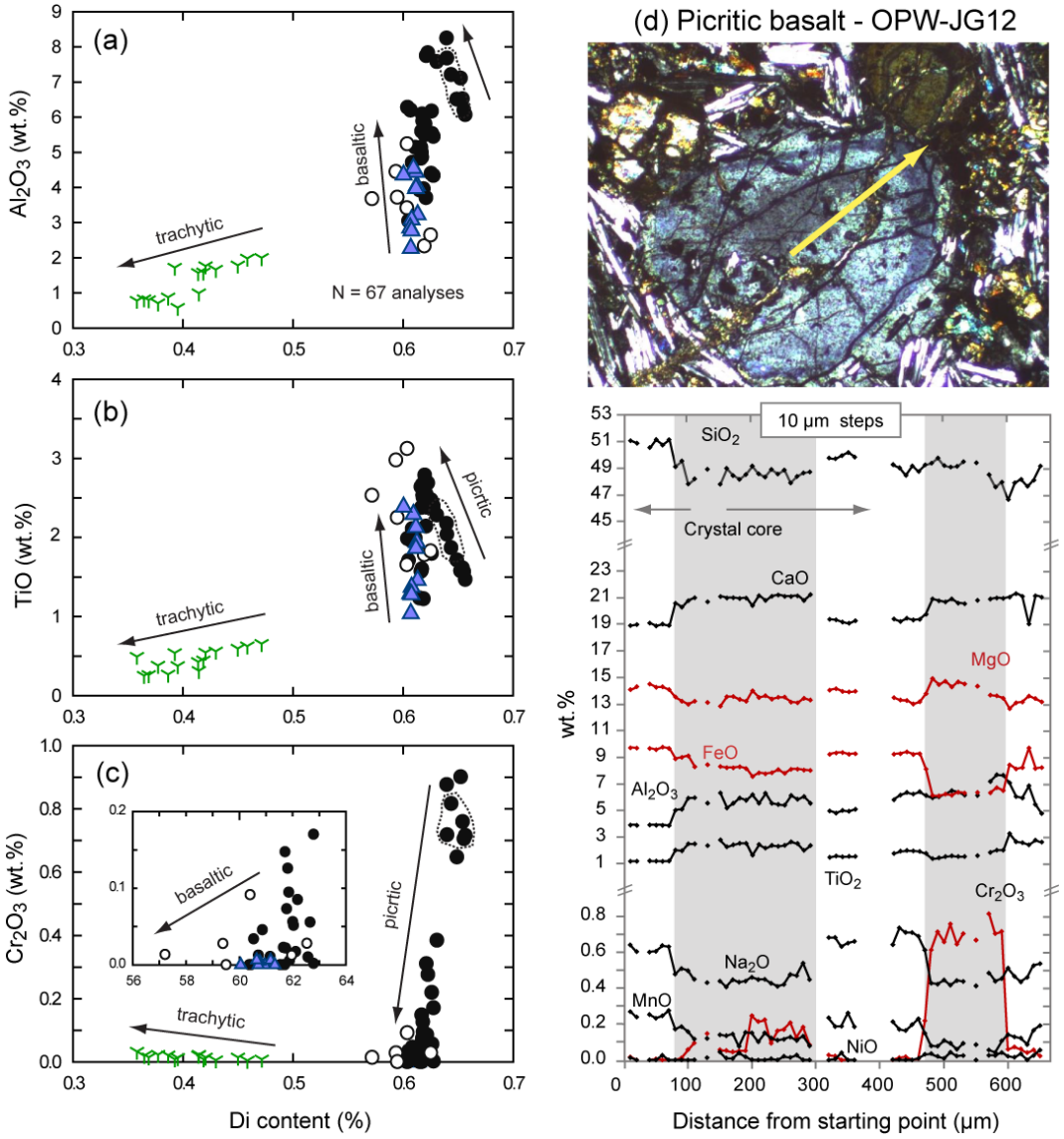

Fig. 12: Clinopyroxene compositions in lavas from Akaroa Volcano. (a) TiO_2, (b) Al_2O_3 and (c) Cr_2O_3 are plotted against Di content. Four trends can be distinguished: (1) Increasing TiO_2 and Al_2O_3 in mafic lavas with decreasing Di contents, (2) Decreasing TiO_2 and Al_2O_3 in trachytic lavas with decreasing Di contents, (3) Decreasing Cr_2O_3 in mafic lavas with decreasing Di content and (4) increasing Cr_2O_3 in trachytic lavas with decreasing Di content. Dashed lines mark growth bands in clinopyroxene phenocrysts from picritic lavas. (d) Core-to-rim profile of clinopyroxene in picritic basalt with an interval of 10 µm. A distinct growth band contains Cr_2O_3 concentrations of up to ~0.8 wt.%. Symbols are as in Figure 13.

Feldspar

Representative microprobe analyses of feldspar are presented in Table 5. For ternary feldspar classification, analyses were re-calculated for 32 apfu (Atoms Per Formula Unit) oxygen.

Compositional variation of feldspar is illustrated in Fig. 13 for the three different rock groups: volcanic rocks, plutonic rocks and mafic enclaves. Detailed mineral traverse are illustrated in Fig.15a-f. Overall, feldspar analyses of Akaroa lavas outline well-defined trends. Normative feldspar constituents of bulk magma are shown for comparison and illustrate slightly different fractionation pathsthan feldspar analyses (i.e. mafic enclaves, trachyte).

Feldspar phenocrysts and microphenocrysts in alkali basalt and hawaiites are typically normally zoned and range in composition from bytownite to labradorite (An_{72-54}). Multiple and oscillatory zoning are common (Fig. 14), but reverse zoning does also occur. Plagioclase microlites display compositions of bytownite with anorthite contents of 61 to 55 %. However, microlite compositions in picritic basalt, have higher anorthite contents of 69 to 66 %. Compared to porphyritic lavas, compositions of plagioclases in aphyric hawaiite exhibit distinctively lower calcium concentrations (An_{49-48}). Moreover, aphyric mugearite composes plagioclase with anorthite contents as low as 20 %. Phenocryst zoning of occasional plagioclase in mugearite shows multiple chemical zones accompanied by dissolution and exsolution of alkali feldspar (Fig. 14). In trachyte, plagioclase and alkali feldspar coexist and converge to a common sodic composition ($An_{48-2}Ab_{50-76}Or_{3-43}$). Feldspars are generally normally zoned and progressively change from andesine to oligoclase to anorthoclase . Some feldspar profiles, however, show multiple zoning between 42 and 8 % anorthite (Fig. 14). In gabbro, plagioclase displays normal oscillatory zoning (Fig.14) similar to patterns in mafic volcanic lavas. However, some core analyses represent higher labradorite compositions of up to 74 % anorthite and show normal zoning trends (An_{74-53}). Schlieren in gabbro contain normally zoned plagioclase that changes from An_{49} to An_{9} and alkali feldspar with compositions of $Ab_{81-60}Or_{14-39}$. Syenite contains reversely and normally zoned bytownite (An_{67-56}). Alkali feldspar coexists and typically forms orthoclase crystals (Or_{96}). Feldspar compositions in mafic enclaves become gradually more enriched in albite towards the crystal rim and range from bytownite to andesine ($An_{71-42}Ab_{29-55}$).

Trace element signatures of SrO are plotted against An contents for volcanic rocks, mafic enclaves and plutonic rock in Fig. 15. Two trends can be distinguished in volcanic rocks and mafic enclaves. At first, SrO becomes progressively enriched in plagioclase (< 0.27 wt.%) with decreasing anorthite contents from ~70 to ~40 %. This trend is followed by a second trend as SrO continuously decreases below detection limit (< 0.01 wt.%) in trachytic rocks below An_{40}. Although trends are less distinguished, plutonic rocks show an increase of SrO (< 0.22 wt.%) with decreasing anorthite contents followed by a decrease in SrO below An_{45}.

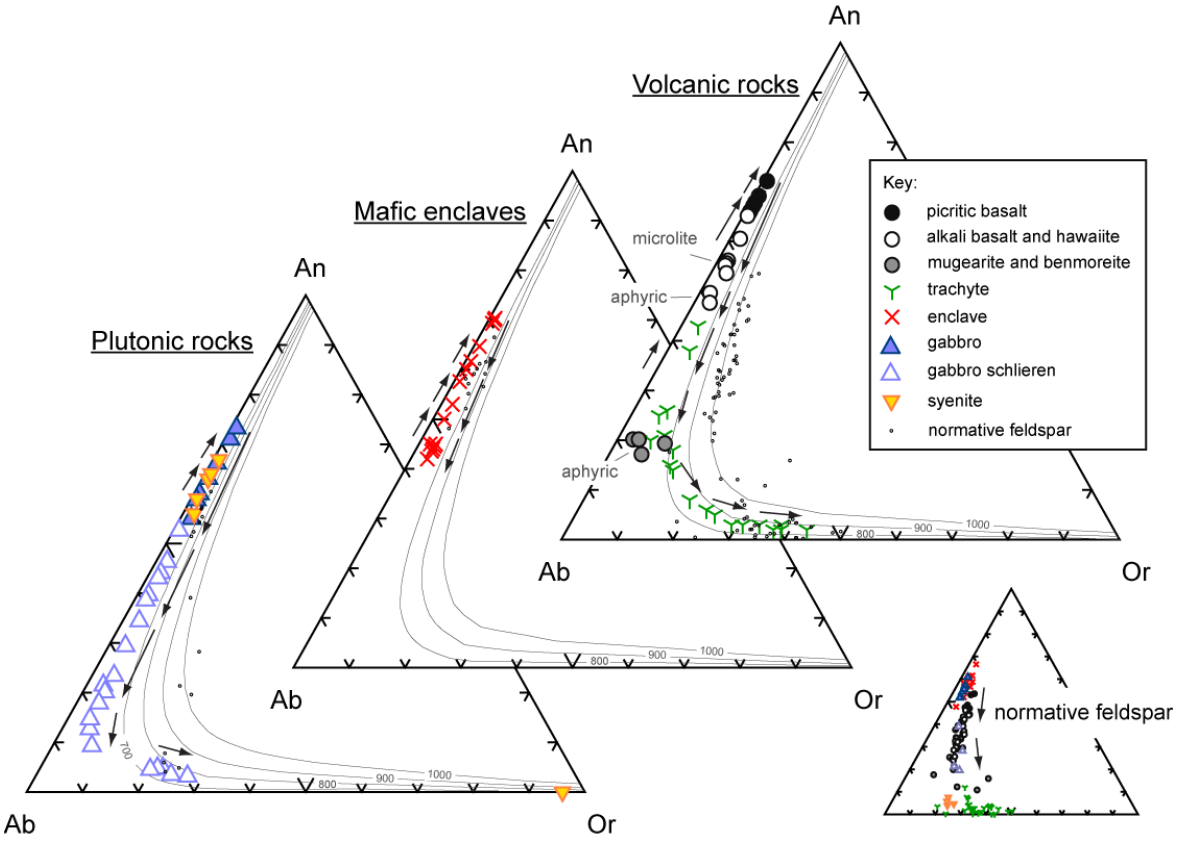

Fig. 13: Selected feldspars and normative feldspar constituents of bulk magma from volcanic rocks, plutonic rocks and mafic enclaves are plotted in the ternary system of An-Ab-Or. The black arrows indicate the feldspar line-of-decent from high to lower temperature feldspars. Normative feldspar constituents of bulk magma are plotted in the corresponding diagram for comparison.

Table 5: Representative analyses of plagioclase in volcanic rocks, plutonic rocks and mafic enlaves

Rock type:	Picritc basalt		Alkali basalt					Hawaiite				Mugearite	
Sample:	*OPW-JG12*	*OPE-JG25*	*OPW-EH1*					*OPE-JG8*			*OPE-JG1*	*OPE-EH1*	
Size:	*mc*	*mc*	*ph-c*	*ph-i*	*ph-r*	*mc*	*mc*	*ph-c*	*ph-r*	*Mc*	*Mc*	*mc*	*mc*
SiO_2	50.89	51.44	54.75	50.27	51.66	54.54	52.54	54.24	51.38	54.17	55.15	62.96	62.93
Al_2O_3	30.89	30.31	28.20	30.39	30.01	28.41	29.74	27.99	30.37	28.89	27.40	22.17	22.62
FeO	0.61	0.86	0.37	0.59	0.48	0.53	0.70	0.29	0.23	0.35	0.99	0.29	0.20
CaO	14.02	13.45	10.81	14.00	13.41	11.11	12.47	11.03	13.29	11.53	9.86	4.16	4.19
Na_2O	3.44	3.76	4.98	3.51	4.06	4.84	4.29	4.97	3.89	4.68	5.34	8.38	8.79
K_2O	0.22	0.23	0.40	0.18	0.24	0.30	0.15	0.44	0.20	0.34	0.36	1.70	0.78
SrO	0.09	0.17	0.21	0.10	0.11	0.15	0.12	0.24	0.19	0.23	0.14	0.12	0.11
Total	100.16	100.22	99.71	99.04	99.97	99.86	100.01	99.19	99.55	100.18	99.24	100.33	99.63
	$An_{69}Ab_{30}$	$An_{66}Ab_{33}$	$An_{53}Ab_{44}$	$An_{68}Ab_{31}$	$An_{64}Ab_{35}$	$An_{55}Ab_{43}$	$An_{61}Ab_{38}$	$An_{54}Ab_{44}$	$An_{65}Ab_{34}$	$An_{57}Ab_{42}$	$An_{49}Ab_{49}$	$An_{19}Ab_{71}$	$An_{20}Ab_{76}$

Table 5: Continued

Rock type:	Trachyte							Gabbro			Syenite		Mafic enclaves	
Sample:	*OPE-NK2*				*3252*			*OPE-JG13*	*OPE-JG13*	*OPE-JG5*	*OPE-JG12*		*HB-RT4*	*HB-RT3*
Size:	*ph-c*	*ph-i*	*ph-r*	*Mc*	*ph-c*	*ph-r*	*mc*	*ph-c*	*ph-r*	*Mc*	*ph-c*	*ph-r*	*ph-c*	*ph-r*
SiO_2	60.62	*57.45*	62.88	64.63	61.45	62.76	66.18	49.01	53.32	53.02	51.09	53.56	49.77	56.90
Al_2O_3	24.92	*26.72*	22.59	20.45	23.52	22.57	19.34	32.08	29.31	29.28	30.35	28.53	31.33	26.12
FeO	0.16	*0.14*	0.22	0.46	0.22	0.25	0.78	0.43	0.46	0.35	0.25	0.32	0.31	0.21
CaO	6.56	*8.68*	4.07	1.80	5.21	3.75	0.58	14.99	11.71	12.02	13.54	11.15	14.79	8.80
Na_2O	6.82	*6.09*	8.50	6.29	7.89	8.21	7.52	2.86	4.45	4.56	3.61	4.67	3.20	6.36
K_2O	0.71	*0.55*	1.08	6.24	0.88	1.84	5.42	0.11	0.22	0.21	0.18	0.27	0.13	0.56
SrO	0.18	*0.22*	0.07	0.09	0.19	0.13	0.00	0.14	0.18	0.11	0.09	0.14	0.17	0.27
Total	99.97	*99.87*	99.41	99.96	99.36	99.50	99.82	99.62	99.65	99.55	99.11	98.64	99.70	99.21
	$An_{33}Ab_{63}$	$An_{43}Ab_{54}$	$An_{20}Ab_{74}$	$Ab_{55}Or_{36}$	$An_{25}Ab_{70}$	$An_{18}Ab_{71}$	$Ab_{66}Or_{31}$	$An_{74}Ab_{26}$	$An_{59}Ab_{40}$	$Ab_{59}Or_{40}$	$An_{67}Ab_{32}$	$An_{56}Ab_{42}$	$An_{71}Ab_{28}$	$An_{42}Ab_{55}$

Abbreviations: ph – phenocryst, mph – microphenocryst, mc – microlite, c – core, i – intermediate, r – rim, An – Anorthite, Ab – Albite, Or – Orthoclase; Oxides are listed in wt.%; $An_{xx}Ab_{xx}$ and $An_{xx}Ab_{xx}$ in mol %.

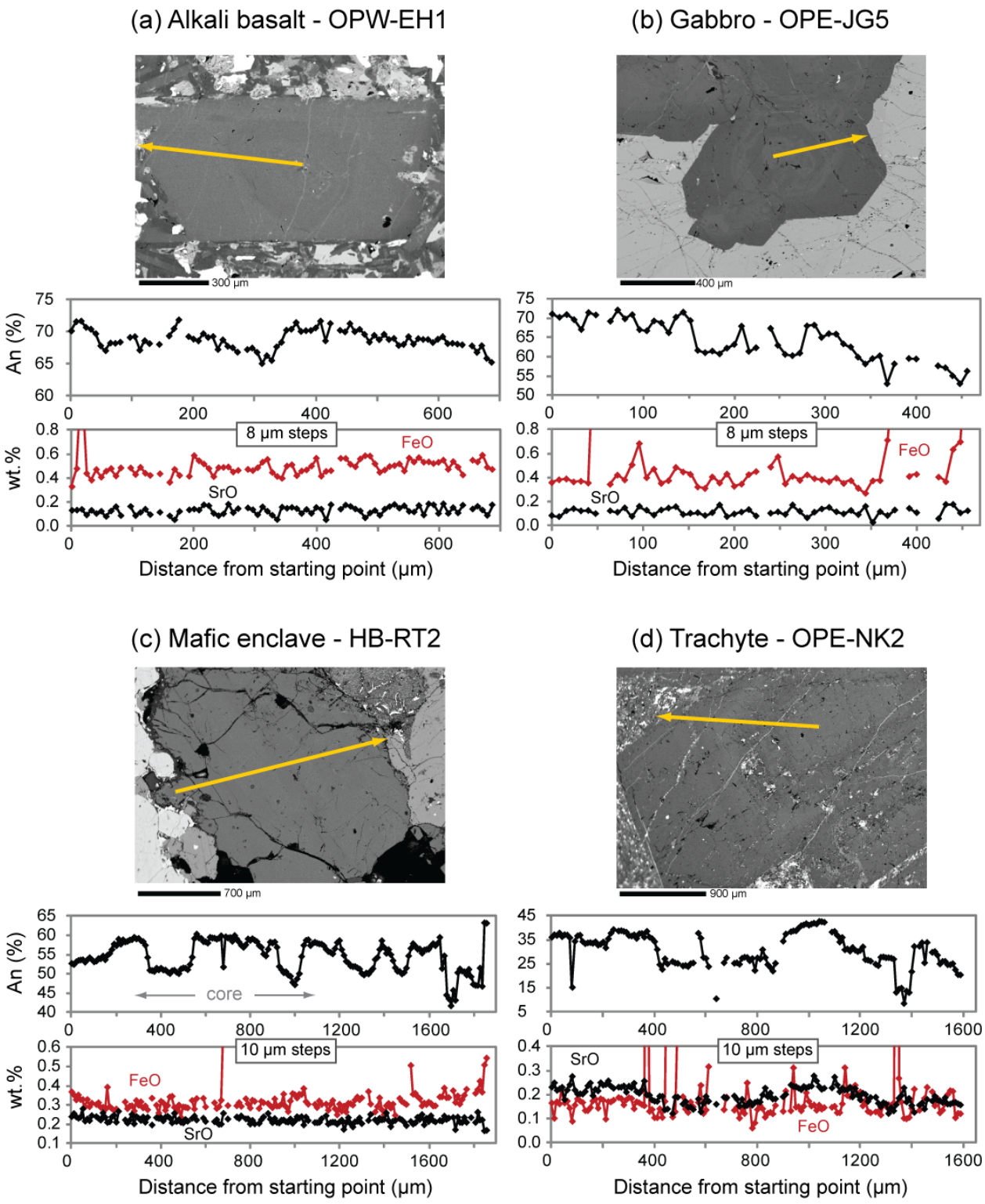

Fig. 14: High resolution microprobe core-to-rim profiles of plagioclase in (a) alkali basalt, (b) gabbro, (c) mafic enclave, (d) trachyte, (e) mugearite and (f) gabbro schlieren. Variations of anorthite, FeO and SrO are plotted against the distance from the starting point (in steps of 8 or 10 µm). Location of the mineral traverses is indicated by yellow arrows on SEM photographs.

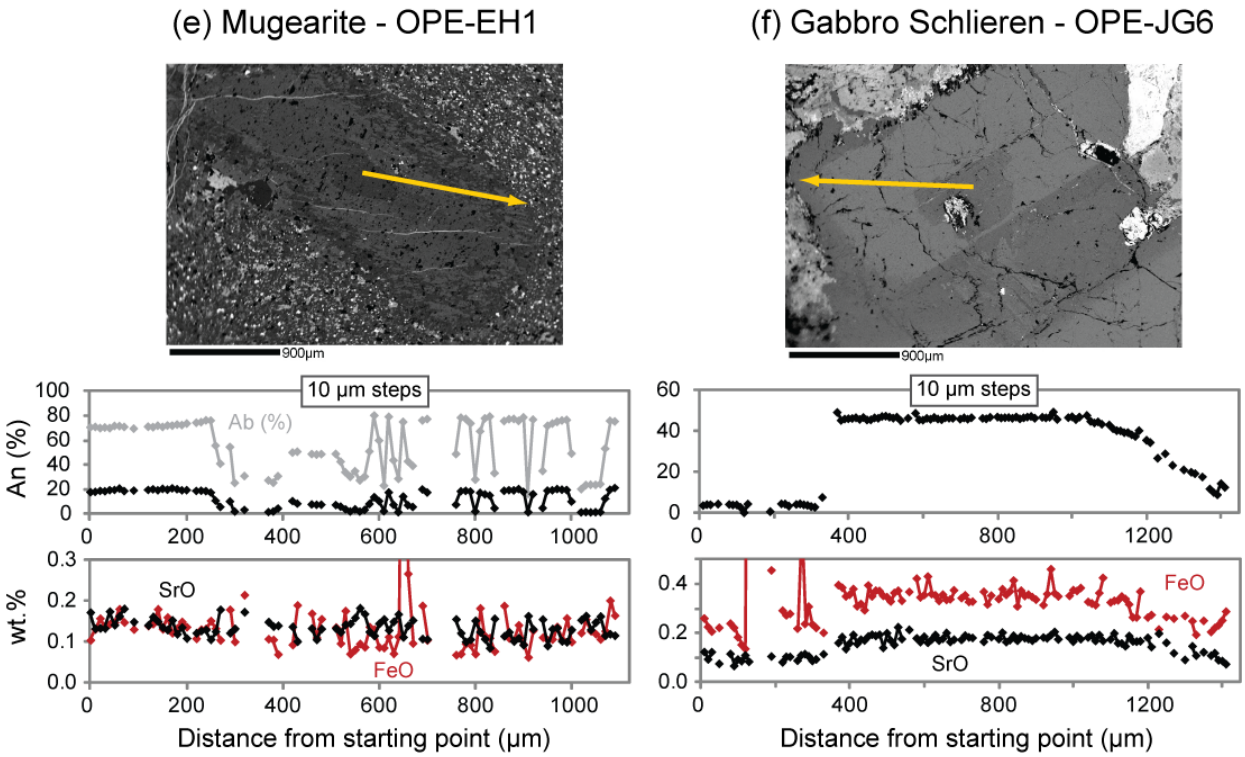

Fig. 14: Continued.

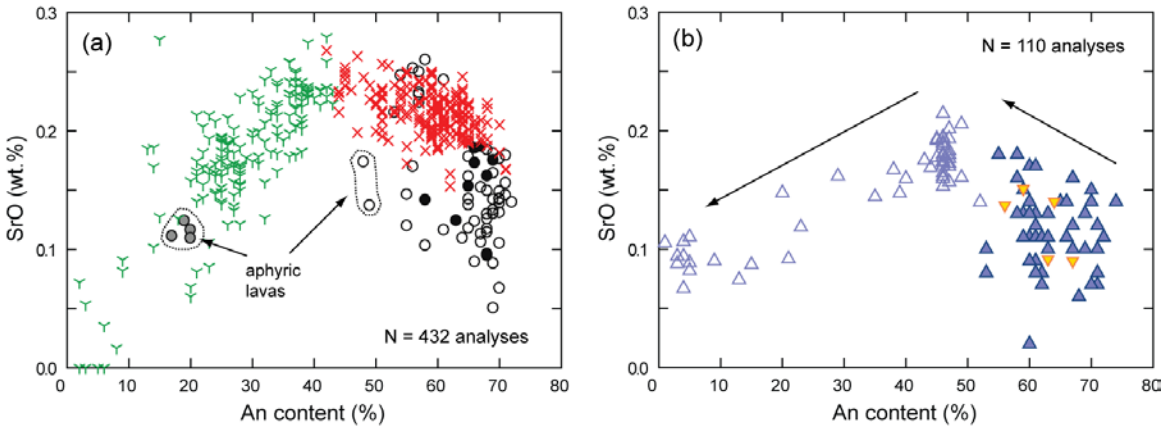

Fig. 15: Feldspar compositions are plotted in variation diagrams showing SrO vs. An content: (a) volcanic rocks and mafic enclaves and (b) plutonic rocks. Dashed lines in (a) indicate aphyric lavas. The black arrows in (b) indicate the fractionation paths of feldspars. Symbols are as in Figure 13.

Amphibole

Amphibole phenocrysts occur only in the gabbro and in some trachyte dikes along Onawe Peninsula. Variations in major elements of amphiboles are recorded in Table 6. All amphibole

analyses were recalculated for Fe^{3+} and classified after Leake (1997). Amphiboles in trachyte vary from potassian hastingsitic hornblende to potassian titanian hastingsitic hornblende – hastingsite and are characterized by high FeO and low MgO contents. Higher MgO and lower FeO contents mark the composition of amphiboles in gabbro, which transit from titanian ferroan pargasite – ferroan pargasitic hornblende into titanian magnesian hastingsite- hastingsitic hornblende.

Compared to amphibole in gabbro, major oxides of amphibole in trachyte are typically lower in SiO_2, TiO_2, Al_2O_3, MgO, CaO, Na_2O, but higher in FeO, MnO and K_2O (Fig. 16). Crystals in trachyte become progressively more enriched in TiO_2 (1.71 – 3.01 wt.%), Al_2O_3 (8.67 – 10.52 wt.%), MgO (0.66 – 2.13 wt.%) and CaO (9.43 – 10.3 wt.%) towards the crystal rim (Fig. 16), Contemporaneously, FeO contents decrease from 33.14 to 29.58 wt.%. The opposite effect occurs in gabbro with TiO_2, Al_2O_3, MgO and CaO contents decreasing from 4.43 to 2.32 wt.%, 11.35 to 9.77 wt.%, 11.35 to 9.56 wt.% and from 11.56 to 10.46 wt.%, respectively. FeO increases from 14.82 – 19.1 wt.% (Table 6). An increase in Cl from 0.04 to 0.21wt.% and a decrease in F from 0.29 to 0.08 wt.% is observed in gabbro. Concentrations of Cl and F in trachyte range between 0.07 and 0.16 wt.% and 0.00 and 0.06 wt.%, respectively. MnO contents gradually decrease from 0.85 to 0.56 wt.% in trachyte and from 0.25 to 0.13 wt.% in gabbro.

Biotite

Biotite is found as phenocrysts in the gabbro and trachyte sill on Onawe Peninsula. For the latter, however, analyses are not made. Representative analysis of biotite in gabbro is presented in Table 6. Chemical data of biotite in gabbro indicates a small substitution of K_2O by Na_2O (< 0.87 wt.%) and high abundance of TiO_2 (< 6.75 wt.%).

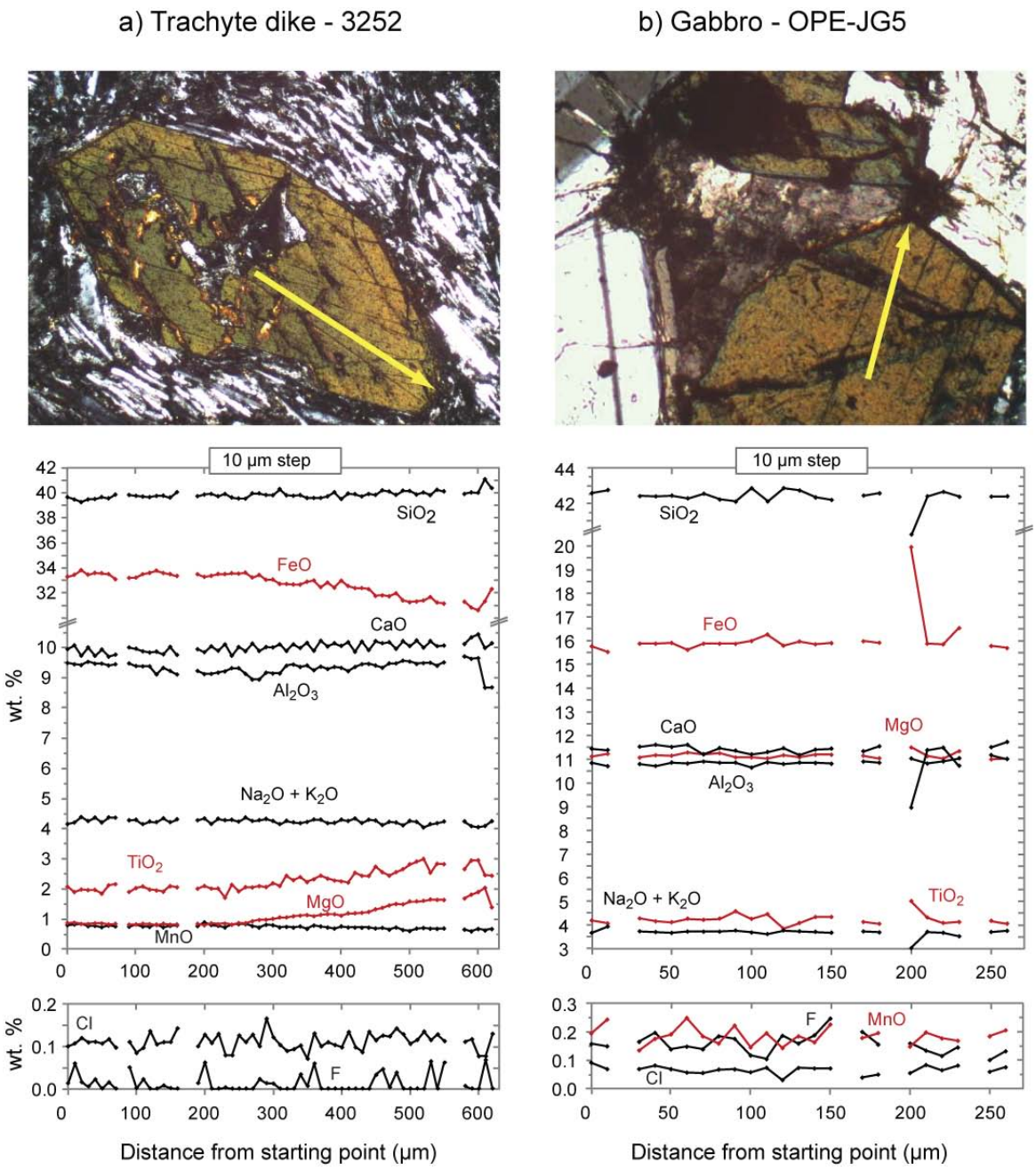

Fig. 16: Core-to-rim microprobe profiles of amphibole phenocrysts from Akaroa Volcano. (a) Amphibole in trachyte displays high FeO and low MgO contents that gradually decrease and increase towards the crystal rim, respectively. TiO_2 concentrations increase rimwards. (b) Amphibole in gabbro is depleated in FeO and enriched in MgO and TiO_2 respectively to trachyte.

Table 6: Representative analyses of amphibole and biotite in trachyte and gabbro

Rock type:	Trachyte - amphibole				Gabbro – amphibole				Gabbro - biotite	
Sample:	*3148*				*OPE-JG5*				*OPE-JG5*	
Size:	*ph-c*	*ph-r*	*ph-c*	*ph-r*	*ph-c*	*ph-r*	*ph-c*	*ph-r*	*ph-c*	*ph-r*
SiO_2	38.54	39.16	38.40	39.37	41.80	45.68	42.22	42.69	37.21	36.92
TiO_2	1.90	2.86	1.71	2.78	4.32	2.32	4.34	2.61	6.75	5.86
Al_2O_3	9.24	9.44	9.25	10.52	11.08	10.96	9.97	9.99	12.80	12.80
FeO	32.77	29.98	33.06	29.66	14.82	15.26	15.24	17.39	18.52	19.04
MnO	0.74	0.64	0.77	0.59	0.19	0.13	0.20	0.17	0.11	0.10
MgO	0.82	1.83	0.66	1.65	11.12	9.96	11.35	10.70	12.04	11.69
CaO	9.48	10.20	9.84	9.99	11.35	10.68	11.24	10.87	0.00	0.03
Na_2O	2.71	2.54	2.66	2.40	2.86	2.86	2.70	2.72	0.86	0.65
K_2O	1.53	1.40	1.55	1.47	0.82	0.42	1.02	0.65	8.53	8.68
Cl	0.11	0.08	0.13	0.09	0.04	0.21	0.05	0.19	0.10	0.10
F	0.02	0.00	0.01	0.06	0.17	0.08	0.14	0.15	0.23	0.14
Total	97.82	98.12	98.02	98.54	98.49	98.48	98.39	98.02	97.04	95.93
				Structural formulae						
Si	6.254	6.302	6.250	6.270	6.229	6.716	6.304	6.374	-	-
Al	1.746	1.698	1.750	1.730	1.771	1.284	1.696	1.626	-	-
∑(T site)	*8*	*8*	*8*	*8*	*8*	*8*	*8*	*8*	-	-
Al	0.021	0.093	0.024	0.245	0.175	0.616	0.058	0.132	-	-
Ti	0.232	0.347	0.209	0.334	0.484	0.257	0.487	0.293	-	-
Fe^{3+}	0.796	0.315	0.715	0.371	0.021	0.000	0.092	0.518	-	-
Fe^{2+}	3.651	3.720	3.785	3.580	1.826	1.876	1.811	1.653	-	-
Mn	0.101	0.087	0.107	0.079	0.024	0.017	0.025	0.022	-	-
Mg	0.198	0.439	0.160	0.392	2.470	2.183	2.526	2.382	-	-
∑(M1-3 site)	*5*	*5*	*5*	*5*	*5*	*5*	*5*	*5*	-	-
Ca	1.648	1.759	1.716	1.705	1.812	1.682	1.798	1.739	-	-
Na	0.352	0.241	0.284	0.295	0.188	0.318	0.202	0.261	-	-
∑(M4 site)	*2*	*2*	*2*	*2*	*2*	*2*	*2*	*2*	-	-
Na	0.500	0.551	0.556	0.445	0.639	0.497	0.579	0.527	-	-
K	0.316	0.287	0.322	0.298	0.155	0.078	0.195	0.124	-	-
∑(A site)	*0.816*	*0.838*	*0.877*	*0.743*	*0.795*	*0.575*	*0.774*	*0.651*	-	-
F	0.011	0.000	0.004	0.033	0.081	0.038	0.066	0.072	-	-
Cl	0.030	0.021	0.036	0.025	0.011	0.051	0.013	0.047	-	-
OH*	1.959	1.979	1.960	1.942	1.908	1.910	1.921	1.881	-	-
∑(OH site)	*2*	*2*	*2*	*2*	*2*	*2*	*2*	*2*	-	-
Sum cations	15.816	15.8380	15.8773	15.7427	15.7945	15.5233	15.7737	15.6511	-	-

Abbreviations: ph – phenocryst, c – core, r – rim, oxides are listed in wt.%, structural formula units are listed in apfu (Atom Per Formula Unit).

Table 7: Representative analyses of Fe-Ti oxides in volcanic and plutonic rocks

Rock type:	Picritic basalt			Alkali basalt		Hawaiite			Trachyte	Gabbro		Syenite	
Sample:	*OPW-JG12*		*OPE-JG26*	*OPW-EH1*		*OPE-JG25*		*OPE-JG1*		*OPE-JG5*		*OPE-JG12*	
Detail:	*il*	*mag*	*mag*	*il*	*mag*	*mag*	*mag*	*mag*	*mag*	*il*	*mag*	*mag*	*ru*
SiO_2	0.05	0.04	0.08	0.02	0.03	0.06	0.05	0.06	0.26	0.00	0.07	0.12	0.01
TiO_2	51.93	24.28	25.29	52.28	26.45	25.40	23.53	22.06	9.20	52.18	15.37	18.57	94.78
Al_2O_3	0.06	2.08	3.28	0.05	1.81	1.88	3.66	2.05	0.59	0.08	4.17	0.07	0.00
Cr_2O_3	0.04	0.27	1.70	0.00	0.10	0.09	0.09	0.01	0.04	0.01	0.02	0.00	0.00
FeO	41.31	65.99	60.80	42.58	64.41	65.73	65.28	67.80	81.14	43.06	73.57	74.62	1.21
MnO	0.62	0.71	0.61	0.57	0.65	0.71	0.65	0.87	1.04	0.61	0.19	0.93	0.00
NiO	0.00	0.08	0.02	0.01	0.02	0.00	0.01	0.01	0.01	0.04	0.02	0.00	0.00
MgO	4.69	1.25	2.81	2.89	1.55	2.68	3.03	2.43	0.04	2.92	0.26	0.07	0.00
ZnO	0.00	0.17	0.14	0.03	0.14	0.10	0.11	0.10	0.30	0.05	0.18	0.59	0.00
Nb_2O_5	0.13	0.01	0.06	0.08	0.00	0.04	0.00	0.02	0.14	0.06	0.00	0.16	4.83
Total	98.83	94.89	94.79	98.51	95.15	96.69	96.39	95.42	92.77	99.01	93.86	95.13	100.84

Abbreviations: il – ilmenite, mag – magnetite, ru – rutile.

Fe-Ti oxide

Representative analyses of Fe-Ti-oxides are presented in Table 7. Titaniferous magnetite is the most common Fe-Ti oxide. Ilmenite – magnetite pairs (Fig. 17) occur in picritic basalt, alkali basalt and gabbro. However, the occurrence of exsolution lamellae (Fig. 17) indicates disequilibrium conditions. Ilmenite compositions are fairly constant in picritic basalt, alkali basalt and gabbro with slightly higher MgO contents in picrititc basalt. Titaniferous magnetite compositions vary significantly from mafic to felsic rock types with TiO_2 contents gradually decreasing (27.42 – 9.2 wt.%) from alkali basalt, picritic basalt, hawaiite, gabbro, syenite to trachyte. Contents of MgO are high in mafic rocks (< 3.03 wt.%) and low in felsic samples (< 0.27 wt.%). Cr_2O_3 (< 1.78 wt.%) is enriched in picritic basalt, while FeO (< 81.14 wt.%), MnO (< 1.38 wt.%) and ZnO (< 1.36 wt.%) contents are enriched in trachyte. Titaniferous magnetite in gabbro contains Al_2O_3 of up to 4.17 wt.% and rutile in syenite represents the highest Nb_2O_5 abundance of 4.83 wt.%.

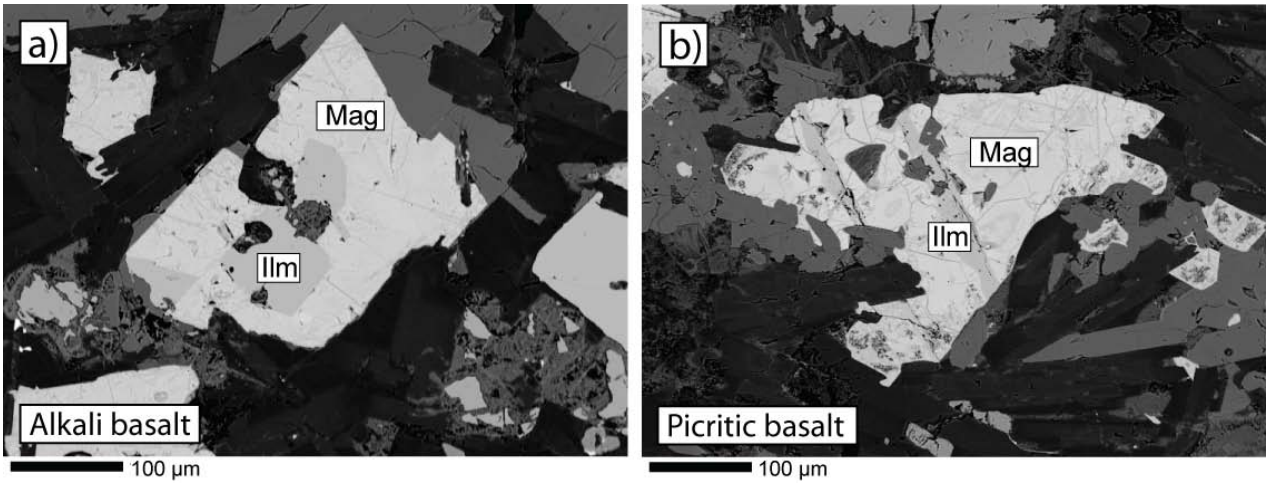

Fig. 17: Magnetite (white) and ilmenite (light grey) pairs in alkali basalt (a) and picritic basalt (b).

MAGMATIC CONDITIONS

Changes in pressure (P), temperature (T) and oxygen fugacity strongly influence the crystallisation history (liquid-line-of-decent) and mineral compositions in magmatic systems. Therefore, evaluating the thermodynamic parameters from activity models using mineral compositions is critical to reconstruct the magmatic history of the Akaroa Volcano. In order to estimate the emplacement/storage depths and thermal evolution of these magmas in the crust, P-T calculations were performed using microprobe analyses of various mineral (i.e. amphibole, plagioclase, clinopyroxene) and thermodynamic activity models (Hammarstrom and Zen 1986; Hollister et al. 1987; Johnson and Rutherford 1989; Schmidt 1992; Anderson and Smith 1995, Holland and Blundy 1994; Ernst and Liu 1998; Putirka 2008).

Clinopyroxene geothermobarometry

Thermobarometers using clinopyroxene compositions alone (Nimis 1995; Nimis and Ulmer 1998; Nimis and Taylors 2000) and clinopyroxene-liquid equilibria (Putirka et al. 1996, 2003) can provide good estimates of crystallisation temperatures and depths. The magnitude of the error associated with P-T estimates can be minimized by obtaining a number of measurements from a particular sample suite. We made a minimum of 9 measurements for each suite (with exception of alkali basalt, N=2) in an effort to improve the resolution of P-T estimates.

The effects of pressure and temperature on clinopyroxene compositions have been recently re-evaluated by Putirka (2008). Pressure estimates from clinopyroxene compositions alone were recalibrated for anhydrous (equation 32a) and hydrous systems (equation 32b) and improved the precision of previous models. The systematic error of anhydrous experiments, however, persists; and to lower the systematic error in anhydrous calibrations the amount of abundant water in the liquid is required to equilibrate the clinopyroxene composition. Temperatures can be estimated from experimental datasets using clinopyroxene compositions as well (equation 32d), but also

imply relatively large uncertainties as equilibrium between mineral and melt is frequently not achieved. In contrast, activity models that determine the chemical equilibrium of two co-existing phases (i.e. crystal-liquid) provide a more accurate calibration scheme and P-T estimates by diminishing the error of the mean value.

Existing clinopyroxene-liquid geobarometers have been (1) recalibrated after the Putirka et al. (1996; equation 30) and (2) recalibrated based on global regression analyses of experimental data with P, T and composition as dependent variables (equation 31). A new barometer based on the Al-partitioning between clinopyroxene and liquid has also been introduced by Putirka (2008, equation 32d) using data from previous studies. The geothermometer is based on liquid-crystal exchange reactions within the Jadeite-Diopside-Hedenbergite system (Putirka et al. 1996, 2003). New calibrations by Putrika (2008) using experiments performed below pressures of 70 kbar have reduced the previous uncertainty of 52 – 60 °C to about 10 - 20 °C. Equation 34 determines the temperature at which a liquid becomes saturated with clinopyroxene and, hence, acts as a test for equation 33. A test for equilibrium can be conducted based on the Fe-Mg exchange (equation 35), but does not take the Na-Al or Ca-Na exchange into consideration.

P-T estimates for Akaroa lavas were made using the clinopyroxene-only thermobarometer (equation 32a, b and d) for alkali basalt, gabbro and trachyte, rather than the clinopyroxene-liquid thermobarometer, because glass (liquid) is sparse and in poor condition and clinopyroxene are late crystallizing, which precludes the use of the bulk-rock as a nominal liquid composition in equilibrium with clinopyroxene formed on, or near, the liquidus. In contrast, equilibrium conditions between clinopyroxene and the bulk-rock composition can be assumed in picritic basalt with clinopyroxene representing an early crystallisation phase. Thus, the crystal-liquid thermobarometer (equation 30 and 31) could be applied using clinopyroxene core analyses as ‘crystal component’ and the bulk-rock composition as ‘liquid composition’. Importantly, only clinopyroxene phenocrysts that don’t show poikilitic texture (enclosing feldspar lathes) were

chosen for thermodynamic calculations to exclude late crystallising phases of pyroxenes which would not be in chemical equilibrium with the bulk-rock composition.

Overall, the error associated with the clinopyroxene-liquid thermobarometers are smaller than other calibration schemes (Table 8), and are, therefore, preferred whenever good measurements of mineral and liquid can be made. Pressures from barometers that use only clinopyroxene compositions are about 25 % lower, whereas models that use a compilation of global regression analysis and Al-partitioning produce pressures that are 30 to 40 % higher. Temperatures from clinopyroxene-liquid thermometers are 35 °C higher than temperatures from clinopyroxene-only calibration. Results from clinopyroxene geothermobarometers reveal a high pressure and temperature environment for picritic basalt (about 10 kbar and 1240 °C; Table 8). In contrast, alkali basalt, gabbro and trachyte appear to have formed at shallower levels (about 3 to 4 kbar) and lower temperatures (about 1150 °C for alkali basalt and gabbro, and about 965 °C for trachyte). However, as shown with the P-T evaluation of different calibrations, clinopyroxene-only barometers produce much lower pressure values than clinopyroxene-liquid models. Therefore, pressure in alkali basalt and gabbro are more likely to be about 1 kbar higher (about 25 % => 4 to 5 kbar) than calculated values. Moreover, calibrations that use anhydrous conditions will provide more reliable estimates as water content increases with evolving magmas (i.e. trachyte).

Amphibole geothermobarometry

Experimental studies have determined the effect of pressure (Johnson and Rutherford 1989b, Thomas and Ernst 1990, Schmidt 1992) and temperature (Spear 1981; Blundy and Holland 1990; Holland and Blundy 1994) on amphibole compositions. These studies have shown that increasing pressures result in increasing Al-contents through the Al-Tschermak substitution [$Si^{T} + Mg^{M1-M3} = Al^{T} + Al^{M1-M3}$]. Increasing temperatures, however, do not favour an Al-Tschermak substitution. Instead, an increase in Al^{T} (tedrahedral position) is induced by rising temperatures through the

edenite exchange [$Si^T + \square^A = Al^T + (Na + K)^A$; ~ 50%], Ti-Tschermak exchange [$2Si^T + Mn^{M1-M3} = 2Al^T + Ti^{M1-M3}$; ~25-30%] and plagioclase exchange [$Si^T + Na^{M4} = Al^T + Ca^{M4}$;10-15%]. Independent of pressure and temperature, variations in f_{H2O} and f_{O2} are known to have a small effect on the Al-contents of amphibole (Anderson and Smith 1995; Scaillet and Evans 1999).

Geobarometers for felsic magmas are generally well constrained (Hammarstrom and Zen 1986; Hollister et al. 1987; Johnson and Rutherford 1989; Schmidt et al. 1992; Anderson and Smith 1995). However, the use of the Johnson and Rutherford (1989) geobarometer is restricted to rocks containing the full buffering assemblage of quartz, alkali feldspar, plagioclase, hornblende, biotite, iron titanium oxide and titanite; and the model from Anderson and Smith (1995) is limited to temperatures between 600 - 800 °C. The semi-quantitative thermobarometer derived by Ernst and Liu (1998) presents a graphical method to estimate temperatures in mafic magmas and generally compares well with calibrations by Hammarstrom and Zen (1986), Hollister (1987) and Schmidt (1992). The more recent evaluation of amphibole-geothermometers (Anderson 1996; Bachmann and Dungan 2002) shows that the hornblende-plagioclase calibration B of Holland and Blundy (1994) represents the most reliable temperature model. Therefore, combined temperature and pressure estimates for Akaroa samples were established for amphiboles in gabbro and trachyte using the Holland and Blundy thermometer B and pressure calibration by Schmidt (1992) and Anderson and Smith (1995). This calculation scheme has also performed well with the Matahina magmas in New Zealand (Deering 2009) showing good correlation with independent Ti-in-hornblende calibrations (Spear 1981; Féménias et al. 2006). For further comparison, P-T estimates were also obtained after the new amphibole calibration from Ridolfi et al. (2009), which investigates the stability field of amphibole in calc-alkaline magmas of subduction-related systems. This geothermometer is calibrated for low pressures (1 to 3 kbar) and oxygen fugacities around the Nickel-Nickel-Oxide buffer (NNO); There, the interpretation about magmatic conditions is limited, but may show some correlations.

Pressure and temperature estimates from amphiboles in gabbro and trachyte are compared in Table 9 and Table 10. Mean pressure values are around 5.5 to 5.9 kbar for gabbro, and 4.9 to 5.3 kbar for trachyte. Estimates using the calibrations by Johnson and Rutherford (1989) are generally about 1 kbar lower. Negative pressure values were generated for gabbroic amphibole using the Anderson and Smith (1995) calibration scheme and indicate that, similar to results from Féménias et al (2006) and Deering (2009), crystallisation temperatures were above 800 °C. However, amphibole in trachyte produced positive pressure values (4.1 kbar ± 0.04, Table 10),which are similar to the temperatures observed from the Johnson and Rutherford (1989) calibration. Pressure estimates for Ridolfi models were negative for trachtye and signifantly lower than other estimates for gabbro (about 3 kbar), which can be explained by the low pressure calibrations. Temperature estimates for amphiboles in gabbro correlate well between the Al-in-hornblende by Holland and Blundy (1994) and independent Ti-in-hornblende thermometers (986 to 956 °C). Mean values derived from Ridolfi et al (2009) are slightly lower (934 ± 3 °C). Results of trachytic amphibole are between 723 and 754 °C. In contrast, temperatures estimated from the Ti-in-hornblende thermometer exhibit distinctly higher values (872 °C), which are not within the errors of the mean values.

Declining temperature trends are observed for temperature dependent amphibole substitutions for gabbroic amphiboles from core to rim (Fig.18), indicating gradual cooling during crystallisation. Amphiboles in trachyte show an increase in the Edenite-, Ti-Tschermak- and Plagioclase- exchange towards the rim suggesting a reheating event of trachyte prior to eruption (Fig. 18). No clear trends are observed for the Al-Tschermak substitution in gabbro and trachtye, which could indicate near isobaric conditions. However, a decrease in Al^T is displayed in gabbro rim analyses and trachyte overgrowth analyses suggesting a decompression event.

Oxygen fugacity

In the evolved magmas of Akaroa Volcano (i.e. syenite, trachyte) the oxygen fugacity is defined by the buffering mineral assemblage of quartz, fayalite and magnetite (QFM). The oxygen fugacity and iron redox state of alkali basalt and gabbro was estimated after France et al. (2010), using microprobe analyses of plagioclase and clinopyroxene. The method is based on the different partitioning of Fe^{3+} and Fe^{2+} between both minerals and the melt phase. However, the model is unsuitable for magmas with silica contents above 60 wt.% and for high pressures systems (> 5kbar), excluding the picritic basalt of Akaroa Volcano.

Calculations on alkali basalt and gabbro produced oxygen fugacities around the QFM buffer, with errors of ±1 log unit. Alkali basalt is slightly above the QFM buffer where as gabbro tends to have an oxygen fugacity below the QFM buffer.

Water contents

Water contents were not measured directly in this study. However, 'dry' primitive magmas (< 0.5 wt.%) are typical for continental rift environments and likely to dictate the compositional trend of Akaroa Volcano. The abundance and appearance of hydrous mineral phases can also serve as a useful guide for estimating the initial H_2O contents. A number of experiments have shown that amphibole and biotite are only stable when the dissolved H_2O content in the melt is above 3-5 wt.% (Best 2003). Therefore, the absence of evidence of early crystallizing hydrous minerals (i.e. amphibole, biotite) in mafic and intermediate (< 60 wt.% SiO_2) volcanic rocks further indicates initial water contents are less than 4wt.% H_2O. Importantly, the relative abundance of subhedral amphibole and biotite does not present an early crystallisation phase in gabbro, but a late appearance within the last melt fractions.

Table 8: Comparison of calculated P and T conditions after Putirka (2008) using clinopyroxene populations of volcanic and plutonic rocks

Clinopyroxene and clinopyroxene-liquid thermobarometer

Picritic basalt (n=10)

	Eq. 30	*Eq. 31*	*Eq. 32a*	*Eq. 32b*	*Eq. 32c*		*Eq. 32d*	*Eq. 33*
Mean P (kbar)	**10.0 ± 0.5**	13.0 ± 0.5	9.5 ± 1.0	7.5 ± 0.7	13.6 ± 1.2	**Mean T (°C)**	1206 ± 15	**1241 ± 7**
Max (kbar)	10.9	13.8	11.4	9.2	16.1	Max (°C)	1236	1255
Min (kbar)	9.4	12.4	8.3	6.7	12.3	Min (°C)	1196	1232
Water (kbar)	*0.2*	*0.2*	-	*0.2*	*0.2*	Water (wt.%)	-	*0.2*

Equation 32a (clinopyroxene barometer, anhydrous)

		Mean P (kbar)	Max. (kbar)	Min. (kbar)
Picritic basalt	(n=10)	9.5 ± 1.0	11.4	8.3
Alkali Basalt	(n=2)	5.2 ± 1.9	6.6	3.9
Gabbro	(n=9)	2.6 ± 0.6	3.2	1.5
Trachyte	(n=15)	9.6 ± 1.1	11.9	8.3

Equation 32b (clinopyroxene barometer, hydrous)

		Mean P (kbar)	Max. (kbar)	Min. (kbar)	Water (wt.%)
Picritic basalt	(n=10)	7.5 ± 0.7	9.2	6.7	*0.2*
Alkali Basalt	(n=2)	**4.1 ± 2.6**	5.8	2.4	*0.5*
Gabbro	(n=9)	**2.9 ± 0.6**	3.7	2.1	*1*
Trachyte	(n=15)	**2.6 ± 0.9**	3.8	0.7	*3*

Equation 32d (clinopyroxene thermometer, anhydrous)

		Mean T (°C)	Max. (°C)	Min. (°C)
Picritic basalt	(n=10)	1206 ± 15	1236	1196
Alkali Basalt	(n=2)	**1145 ± 33**	1169	1122
Gabbro	(n=9)	**1148 ± 8**	1157	1134
Trachyte	(n=15)	**965 ± 29**	1022	919

Equation 34 (liquid saturation)

		Mean T (°C)	Max. (°C)	Min. (°C)	Water (wt.%)
Picritic basalt	(n=10)	1164 ± 1	1236	1196	*0.2*
Alkali Basalt	(n=2)	1107 ± 21	1131	1042	*0.5*
Gabbro	(n=9)	1107 ± 6	1115	1099	*1*
Trachyte	(n=15)	878 ± 1	879	875	*3*

Equation 35 (equilibrium test)

		KD (Fe-Mg)	Max value	Min value
Picritic basalt	(n=10)	0.294 ± 0.001	0.295	0.292
Alkali Basalt	(n=2)	0.262 ± 0.005	0.267	0.257
Gabbro	(n=9)	0.265 ± 0.003	0.269	0.261
Trachyte	(n=15)	0.204 ± 0.003	0.21	0.197

Table 9: Comparison of calculated pressures using single amphibole populations in gabbro and trachyte

	Hammarstrom & Zen (86)	Hollister et al. (87)	Johnson & Rutherford (89)	Schmidt (92)
Gabbro (OPE-JG5; n=29)				
Mean P (kbar)	**5.5 ± 0.3**	**5.8 ± 0.3**	**4.4 ± 0.2**	**5.9 ± 0.3**
Max (kbar)	6.1	6.4	4.9	6.4
Min (kbar)	4.8	5.0	3.9	5.2
Trachyte (3148; n=62)				
Mean P (kbar)	**4.9 ± 0.3**	**5.1 ± 0.3**	**3.9 ± 0.2**	**5.3 ± 0.2**
Max (kbar)	6.0	6.4	4.9	6.4
Min (kbar)	4.1	4.3	3.3	4.6

Note: Stoichiometric calculations after Leake (1997).

Table 10: Comparison of calculated temperatures and pressures using amphibole populations in gabbro and trachyte

A) Holland and Blundy (1994), Al-in-hornblende thermometer B

Gabbro (OPE-JG5; n=29)			*Trachyte (3148; n=62)*		
XAb=40	*Schmidt (92)*	*Anderson and Smith (95)*	*XAb=90*	*Schmidt (92)*	*Anderson and Smith (95)*
P (kbar)	5.9 ± 0.3	*negative values	P (kbar)	5.3 ± 0.03	4.1 ± 0.3
Mean T (°C)	**979 ± 34**	**963 ± 37**	**Mean T (°C)**	**754 ± 9**	**753 ± 9**
Max (°C)	1009	997	Max (°C)	772	771
Min (°C)	819	795	Min (°C)	716	714
XAb=45	*Schmidt (92)*	*Anderson and Smith (95)*	*XAb=93*	*Schmidt (92)*	*Anderson and Smith (95)*
P (kbar)	5.9 ± 0.3	*negative values	P (kbar)	5.3 ± 0.2	4.1 ± 0.3
Mean T (°C)	956 ± 36	943 ± 36	Mean T (°C)	725 ± 9	724 ± 9
Max (°C)	985	975	Max (°C)	742	742
Min (°C)	797	778	Min (°C)	688	687

B) Féménias et al. (2006), Ti-in-Hornblende thermometer

Gabbro (OPE-JG5; n=29)			*Trachyte (3148; n=62)*		
Mean T (°C)	Max (°C)	Min (°C)	**Mean T (°C)**	Max (°C)	Min (°C)
986 ± 45	1013	854	**872 ± 49**	976	788

C) Ridolfi et al. (2009), calc-alkaline magmas

Gabbro (OPE-JG5; n=28)			*Trachyte (3148; n=62)*		
Mean P (kbar)	Max (kbar)	Min (kbar)	Mean P (kbar)	Max (kbar)	Min (kbar)
2.8 ± 0.2	3.3	2.3	-	-	-
Mean T (°C)	Max (°C)	Min (°C)	Mean T (°C)	Max (°C)	Min (°C)
934 ± 17	951	885	-	-	-

Note: Stoichiometric calculations for A) and B) after Holland and Blundy (1994).

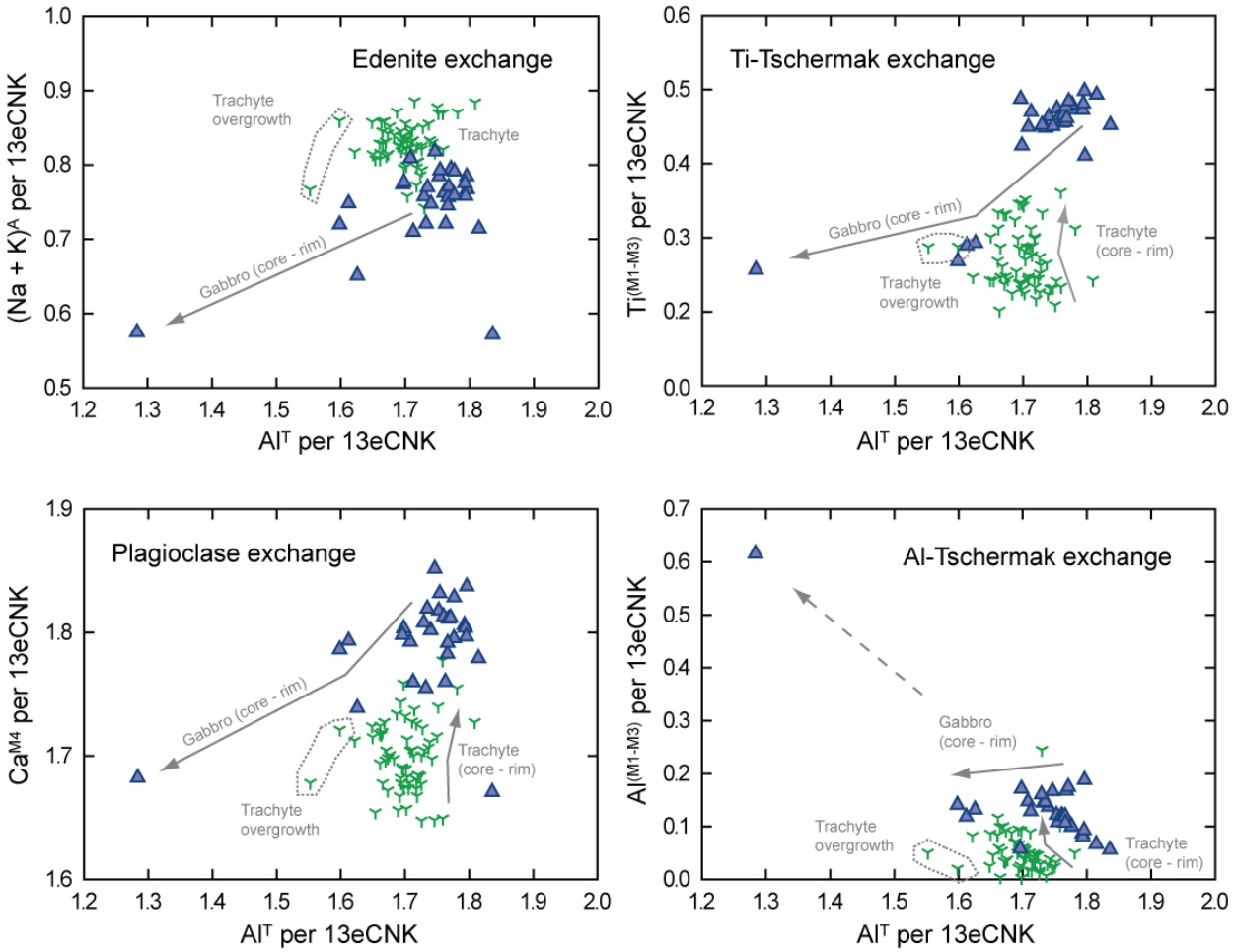

Fig. 18: Temperature dependent substitutions (Edenite, Ti-Tschermak and Plagioclase exchange) and pressure dependent substitution (Al-Tschermak exchange) in analysed amphiboles. For explanations see text. Symbols are as in Figure 13.

DISCUSSION

The following chapters evaluate the magmatic evolution of Akaroa Volcano from the mantle-crust boundary to the surface. In particular, we examine the origin of the "Daly Gap", which exists between the voluminous basaltic lavas that dominate the volcanic structure and subordinate trachytic lavas that occur piecemeal throughout the volcanic history. The major interpretations of this study can be divided into two sections: (1) Basaltic magmastism and (2) trachytic magmatism and a Daly Gap.

BASALTIC MAGMATISM

Primitive magmas and magma ascent

Mafic lavas that were erupted at the surface of Akaroa Volcano generally do not represent primary mantle-derived magmas (Yoder and Tiller 1962, O'Hara 1965). It is more likely that mafic assemblages represent primitive melts that have progressively changed in chemistry during magma ascent.

The most primitive rocks sampled from the central shorelines of Akaroa Harbour are crystal-rich picritic basalts with MgO contents of more than 10 wt.% and Ni concentrations of over 200 ppm (Table 1). According to Hess (1992) these high-Mg rocks could represent near-primary, mantle-derived magmas. However, olivine phenocrysts (Fo_{80-76}) are not in equilibrium with the bulk-rock composition (Mg#: 60) using the olivine-liquid equilibrium test of Roeder and Emslie (1970). On the basis of this observation it can be concluded that no near-primary magmas have been erupted at the surface and that crystal-rich picritic basalts are the result of crystal accumulation, which lead to a more mafic bulk rock composition.

Pressure dependent mineral assemblages

Experimental simulations of incremental crystal fractionation (Nekvasil et al. 2004; Whitaker et al. 2006) have demonstrated that the crystallising mineral assemblages and the resulting liquid line of descent of silica-saturated alkali series rocks are strongly dependent on the pressure conditions and on the initial bulk water content. At high pressures (9.3 kbar), early crystallisation of olivine and clinopyroxene dominates the mineral assemblage; whereas at lower pressures (less than 6.8 kbar), olivine and plagioclase become early crystallising phases.

At high pressures, the initial bulk water content determines whether plagioclase crystallises or not. Under anhydrous conditions (0.05 wt.% bulk H_2O) plagioclase will crystallise in addition to olivine and clinopyroxene causing a relative increase in K_2O in the melt. Consequently, crystal-liquid separation in magmas with low initial water contents will result in higher $K_2O/(Na_2O + K_2O)$ ratios and proceed to differentiate along a potassic trend. If initial bulk water contents are $\geq$ 0.5 wt.%, plagioclase crystallisation is suppressed, which leads to higher $Na_2O/(Na_2O + K_2O)$ ratios and magma differentiation along a more sodic trend.

Two distinctively different mineral assemblages occur in the mafic lavas of Akaroa Volcano: (1) A high-pressure assemblage containing olivine and clinopyroxene phenocrysts; and (2) a low-pressure assemblage containing olivine and plagioclase. By comparing these assemblages and P-T-estimates from crystal-liquid phase equilibria of the natural samples to the experimental studies we can constrain the magmatic conditions including the bulk water content, and subsequently the liquid line of decent of the evolving magmas.

Abundant olivine and clinopyroxene phenocrysts in the picritic basalts of Akaroa Volcano (less than 30% phenocrysts) and related pressure-temperature estimates from the clinopyroxene-liquid compositions (10 ± 0.2 kbar, 1241 ± 2 °C; Table 8) correlate well with the mineral assemblages and temperatures produced from high pressure experiments (9.3 kbar) of anhydrous magmas from the Snake River Plains (Whitaker et al. 2006). In contrast, experimental results on

basalts under relatively wetter conditions (≥ 0.5 wt.% H_2O) from the Nandevar Volcano (Nekvasil et al. 2004), reveal much lower temperatures (1080 °C) at crystallinities of 20 to 30%. Based on this comparison with experiments and geothermobarometery determined on crystal-liquid equilibria, the picritic basalts of Akaroa Volcano are more likely to contain initial bulk water contents below 0.5 wt.% and were produced at depths close to 10 kbar (near the mantle-crust boundary; Thomas and Evison 1962; Wellman and Latter 1989; Sewell et al. 1993).

The mineral assemblages in the more evolved alkali basalt and hawaiites of Akaroa Volcano are consistent with early olivine and plagioclase crystallisation at lower pressures (less than 6.8 kbar, Nekvasil et al. 2004, Whitaker et al. 2006). Forsterite (Fo_{80}) and anorthite contents (An_{70-72}) of olivine and plagioclase phenocrysts of Akaroa lavas, respectively, are also comparable to olivine and plagioclase compositions derived from experiments (Nekvasil et al. 2004; Whitaker et al. 2006). Temperature estimates from clinopyroxene compositions in alkali basalt at Akaroa Volcano (1145 ± 23 °C, Table 8), are lower than temperatures revealed from anhydrous experiments (1200 to 1220 °C, Whitaker et al. 2006) and indicate that alkali basalt and hawaiite fractionated along a relatively wetter liquid line of descent compared to the picritic basalt.

In summary, the phase equilibria of abundant phenocrysts and the geothermobarometric calculations strongly suggest that the picritic basalt fractionated at deep levels, whereas alkali basalt and hawaiite fractionated at shallower levels before reaching the surface.

Fractional crystallisation

Fractional crystallisation (Bowen 1928) has been suggested to play the dominant role in the magmatic evolution of Akaroa Volcano (Price and Taylor 1980). At Akaroa Volcano, petrological observations and the bulk-rock chemistry reinforce the fractional removal of olivine, clinopyroxene, Fe-Ti oxides, plagioclase and apatite to create more evolved daughter compositions (Price and Taylor, 1980). Early fractionation of olivine leads to a decrease in MgO and Ni

concentration, whereas the fractionation of clinopyroxene crystallisation explains decreasing CaO and Cr contents. These compatible fractionation trends also occur in normally zoned olivine (Fig. 9) and clinopyroxene phenocrysts (Fig. 12) supporting fractional crystallisation processes. Early olivine and clinopyroxene fractionation is associated with silica depletion and an enrichment of TiO_2, Al_2O_3 and alkali components (Fig. 5), also recorded in the mineral composition of abundant clinopyroxene. Incompatible behaviour of V from picritic basalt to alkali basalt (Fig. 6) suggests that magnetite crystallisation was suppressed and not involved in the initial Cr fractionation. The abrupt transition from incompatible to compatible behaviour of TiO_2, displayed between picritic basalt and alkali basalt, may be a result of ilmenite crystallisation. If this is the case, alkali basalt must have differentiated at lower temperatures to allow for ilmenite crystallisation (~ 1080 °C, Whitaker et al. 2006). Increasing Sr concentrations from picritic basalt to alkali basalt reinforces the argument that plagioclase was not an early crystallisation phase in the more primitive magmas, consistent with high pressure differentiation experiments (Nekvasil et al. 2004, Whitaker et al. 2007). Feldspar fractionation, on the other hand, dominates the fractionation assemblage of more evolved rocks causing a sharp decrease in Al_2O_3 from picritic basalts to alkali basalt (Fig. 5). Apatite crystallisation occurs at about 49 wt.% SiO_2 causing the inflection of P_2O_5 in SiO_2 vs. P_2O_5 bivariant plot (Fig. 5).

Using pMELTS (Ghiorso et al. 2002), the observed compositional trends of mafic and intermediate rocks cannot be quantitatively reproduced by high pressure fractionation at 10kbar. Extensive crystallisation of clinopyroxene leads to silica depletion and a strong aluminium enrichment (Fig. 19), which is not observed in the natural assemblages. To allow for aluminium depletion plagioclase fractionation is required at shallower depths. Hence, a single stage crystal fractionation model cannot explain the chemical diversity. Below we examine the possibility of an additional stage of crystal fractionation at shallower levels in the crust.

Using MELTS (Ghiorso and Sack 1995), major element variations can be fitted at lower pressures (5kbar) with alkali basalt (i.e. OPW-EH1) and bulk water contents of 0.5 wt.% (Fig. 5).

The oxygen fugacity is set at the quartz-fayalite-magnetite (QFM) buffer. Based on these observations, we propose that crystal fractionation occurred at mid-crustal levels to produce the compositional variation from alkali basalt to hawaiite-mugearite, and ultimately to produce the cogenetic trachytic compositions. Extraction of trachyte from a picritic source falls outside the constrained framework for effective crystal-liquid separation and precludes a single step fractionation model (Fowler and Spera 2010) from picrite to trachyte.

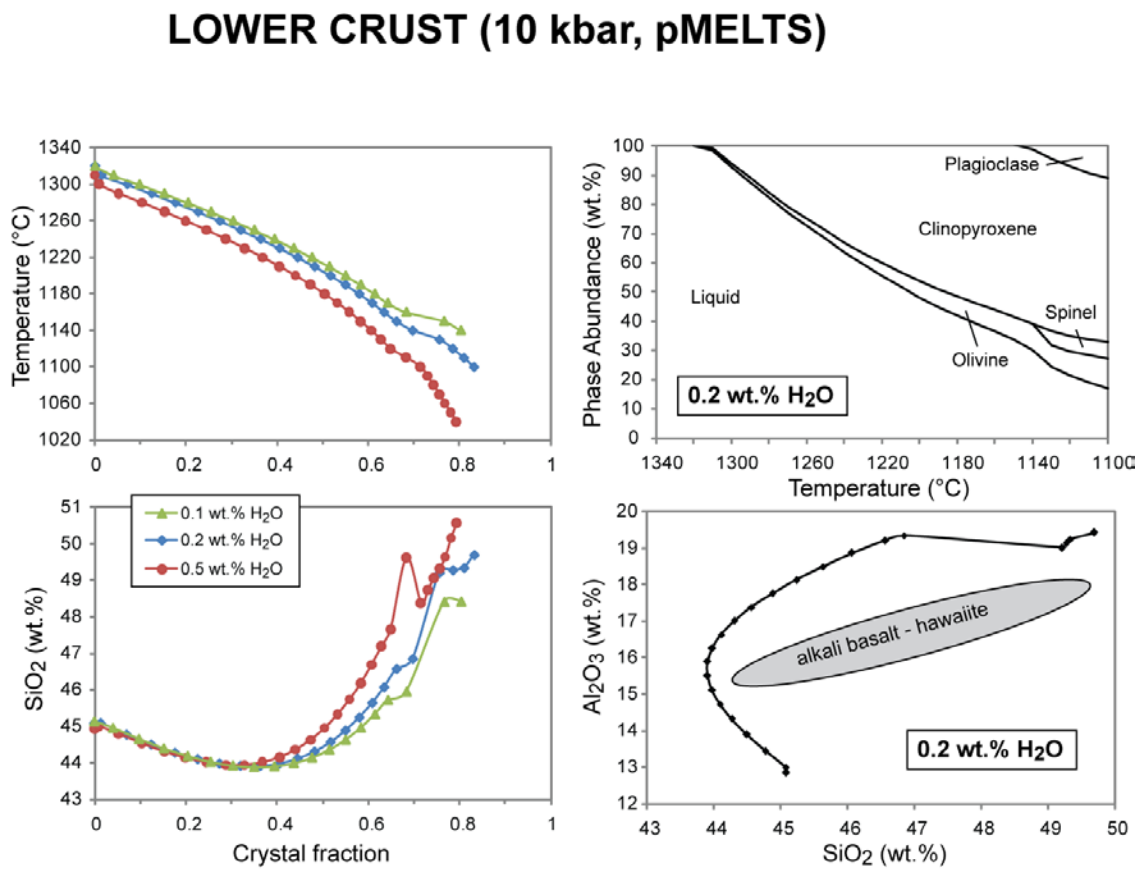

Fig. 19: Crystal fractionation simulations at high pressures 10 kbar using pMELTS (Ghiorso et al. 2002). Temperature and silica variations are illustrated for 0.1, 0.2 and 0.5 wt.% H_2O (left). Clinopyroxene domination is illustrated in the top right. Alumina enrichment is plotted vs silica on the bottom right and compared to natural variations.

THE FORMATION OF TRACHYTE AND A DALY GAP

The geochemical trends that define the Akaroa Volcanic Suite strongly indicate a fractional crystallization origin for trachytic melts (Price and Taylor 1980); however, a distinct compositional gap (i.e. the "Daly Gap") exists between the mafic compositions and the trachyte. Some workers have suggested that this gap arises from the melting of supracrustal rocks (Reference), but, in arc settings, Brophy (1991) suggested that this gap originated from a physical process that limited the extraction to within an optimal crystallinity window. Recently, the physical separation of liquid from crystallising minerals was explored using the numerical models that coupled crystallisation kinetics with multiphase fluid dynamics in magma reservoirs. These indicate that it is most probable that melt extraction will occur within a window of about 50 to 70 vol.% crystals (Dufek and Bachmann 2010). The results of extraction only within this window lead to the formation of compositional gaps of different magnitudes. Therefore, in this section we evaluate the formation of trachyte on the basis of crystal fractionation processes within the well-constrained framework for physical melt extraction (50 – 80 vol.%).

Major element modelling using MELTS

In order to quantitatively test the major element variation from hawaiite to trachyte, we have simulated crystal fractionation with sample OPE-JG8 (Harbour Formation) and water contents of 0.5 to 2 wt.% at pressures of 3 to 5 kbar using MELTS (Ghiorso and Sack 1995, Asimov and Ghiorso 1998). Within the established framework for melt extraction (50 to 80 vol.%) trachytic melts with 59 to 66 wt.% SiO_2 are most likely to erupt. The fractionated assemblage of spinel, plagioclase, orthopyroxene (3 kbar: ≤ 1 wt.% H_2O), clinopyroxene (3 kbar: > 1 wt.% H_2O) and apatite is left in a crystal residue. At 3 kbar, orthopyroxene crystallises with initial water contents of 1 wt.% H_2O or less (Fig. 20), whereas clinopyroxene crystallises if water contents

exceed 1 wt.%. MELTS simulations are consistent with geochemical and petrological observations of natural samples (Fig. 5) and accurately predict the observed Daly Gap.

We have quantitatively illustrated that trachytic melts of Akaroa Volcano can be produced from hawaiite by liquid-crystal separation within an optimal window of 50 to 80 vol.% crystal fraction. In the next chapter, we will test whether we can constrain the analysed trace element concentration using the same principles.

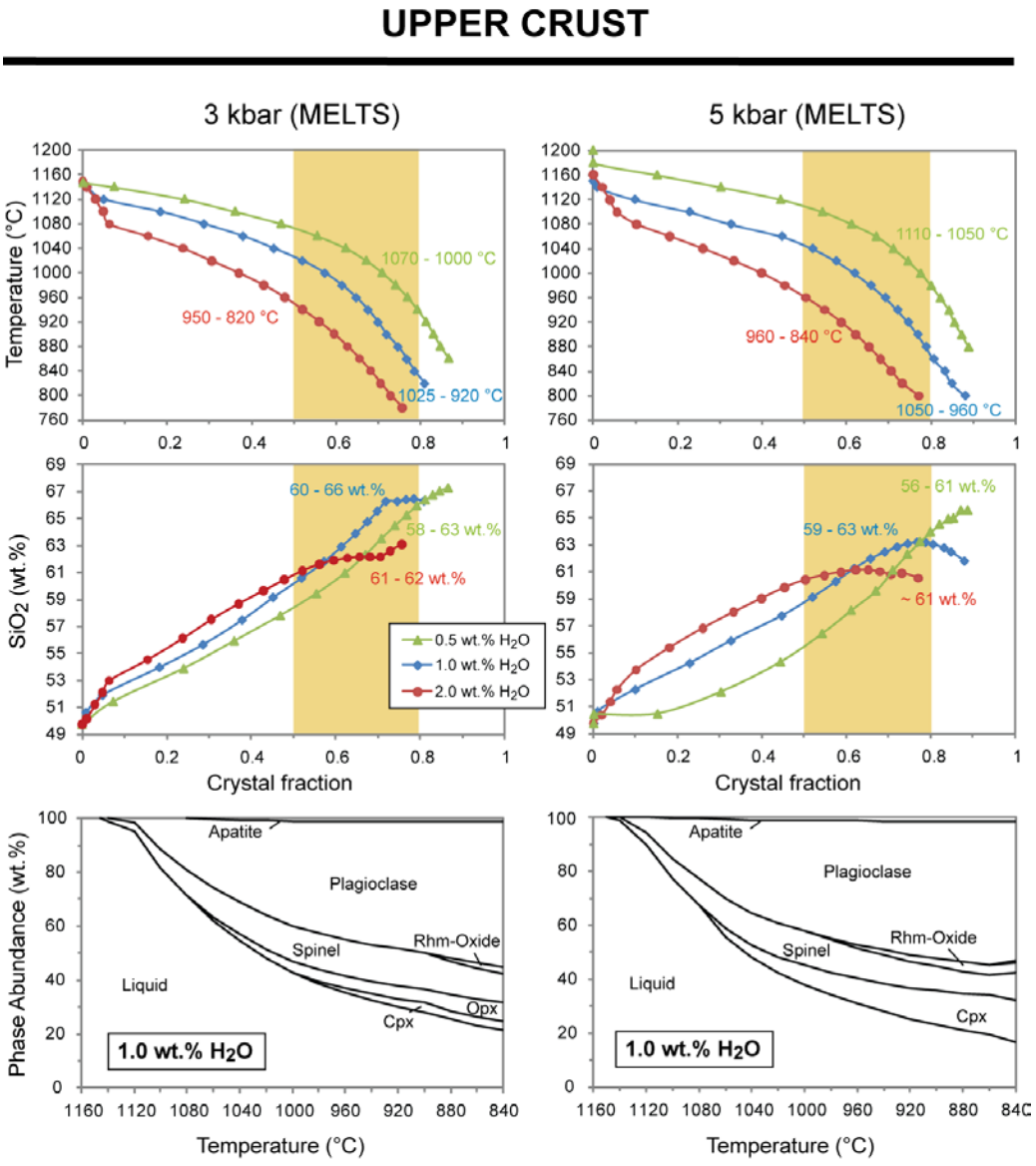

Fig. 20: Crystal fractionation simulations at 3 kbar (left) and 5 kbar (right) using MELTS (Ghiorso and Sack 1995). The upper diagrams shows silica variations with increasing crystallinity for 0.5, 1 and 2 wt.% H_2O. Trachytic melts with silica contents of 58 to 66 wt.% are produced within an extraction window of 50 to 80 vol.% crystals. The bottom diagrams show the crystallising mineral phases with decreasing temperature.

Trace element modelling

Trace elements are more sensitive than major elements to changes in the magmatic conditions. Consequently, the effect of fractional crystallisation processes in evolving magmas can be more pronounced in trace elements than major element data. Deering and Bachmann (2010) have illustrated that if trace element concentrations and bulk partition coefficients are known, trace element models can provide 'good' indicators for crystal accumulation processes. Therefore, by coupling Rayleigh fractionation calculations with the physical processes of melt extraction we can quantitatively predict the concentration of any trace element in the liquid and crystal residue.

In order to test the crystal-liquid separation processes in the more evolved lavas of Akaroa Volcano, we chose two natural samples (OPE-JG8 and OPE-EH1) from the Harbour formation and two key trace elements: Cr (highly compatible) and Rb (highly incompatible). We used the equations provided in Deering and Bachmann (2010):

(1) $C_L = F^{D-1} C_0$ for the liquid component

(2) $C_R = (1-F^D/1-F) C_0$ for the crystal residue

where C_L = concentration in liquid, C_R = concentration in crystal residue, C_0 = concentration in starting material, F = crystal fraction and D = bulk partition coefficient. The bulk rock coefficient is calculated using the phase proportions and partition coefficient of each element: $Di=x_1Kd_1 + x_2Kd_2 = x_3Kd_3$ ....; where i = element; Kd = partition coefficient and x = modal proportions. The partition coefficients used are listed in the supplementary data. Cr concentration of the starting materials were slightly modified from natural samples but have been observed in similar natural samples (i.e. Cr = 21 ppm).

The results of trace element modelling (i.e. Cr and Rb) are in close agreement with the concentrations observed in the trachyte and in co-magmatic inclusions (Fig. 21). This strong

evidence supports the hypothesis that the co-magmatic enclaves from Haylocks Bay represent a cumulate residue from the crystal-liquids separation processes responsible for the formation of trachyte and a Daly Gap at Akaroa Volcano. Results, however, strongly depend on the initial trace element concentration and the element partition coefficient.

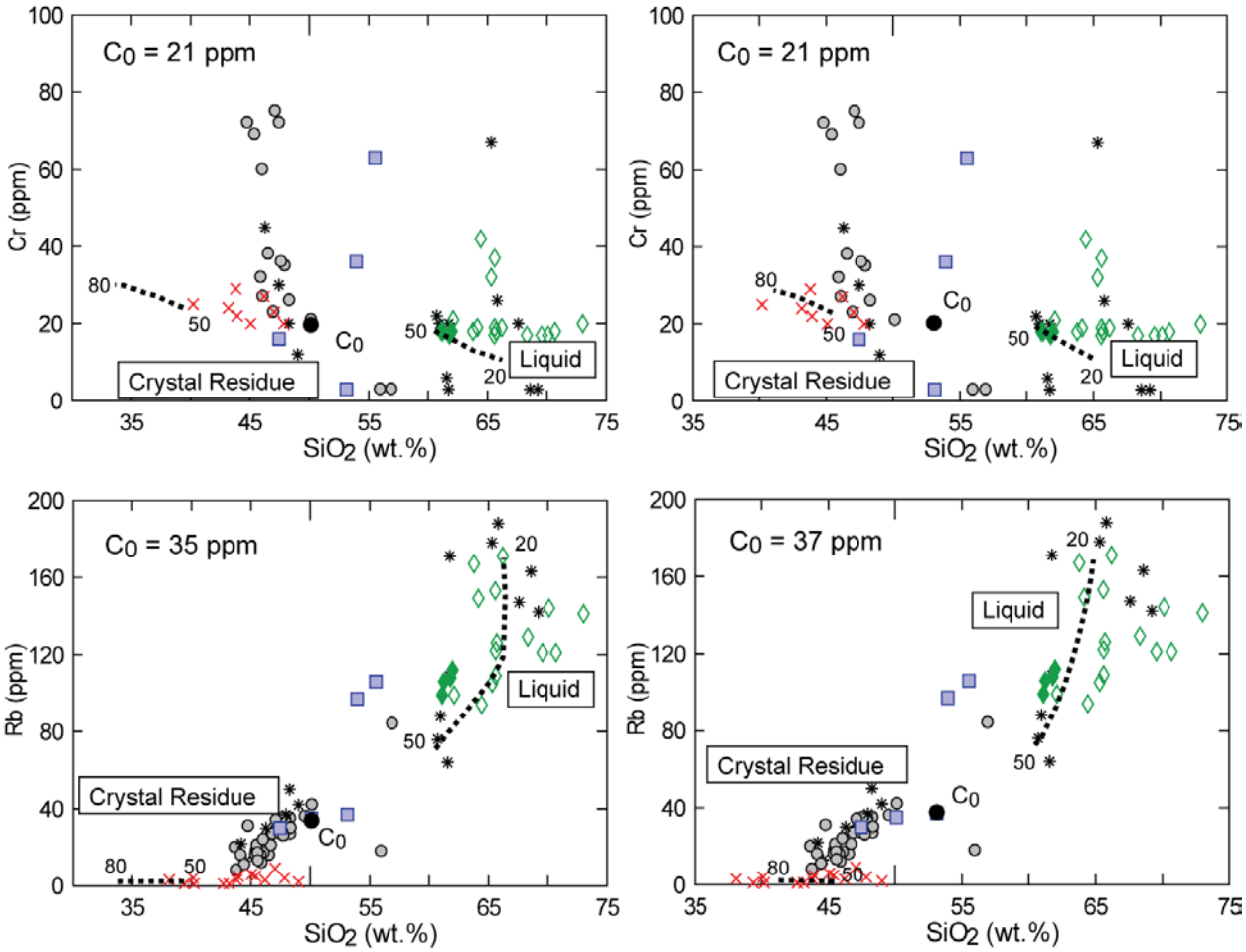

Fig. 21: Trace element modelling of Cr (top) and Rb (bottom) Rayleigh fractionation starting with an initial hawaiite (left) and mugearite (right) composition taken from natural samples. Models use MELTS-derived conditions for crystal fraction between 50 and 80 vol.% (dashed line). The crystal residue (80 to 50 vol%) represent the composition of accumulated crystal after 20 to 50 vol.% melt has been extracted. The liquid represents the composition of melt (20 to 50 vol.%) that has been extracted from an intermediate crystal mush. Symbols are as in Figure 5 and 6.

Mineral records

As shown in the previous two sections, trachyte and co-magmatic enclaves likely represent the product of effective liquid-crystal separation within an optimal extraction window of 50 to 80 %. Therefore, we expect to see a continuous solid solution in the mineral phases of the liquid (i.e. trachyte) and crystal residue (i.e. co-magmatic enclave).

The normative feldspar compositions of gabbroic enclaves and trachyte display two different mineral populations (Fig. 13), an anorthite rich population and an anorthite poor population, respectively. However, analysed plagioclases frame the entire range of compositions from An_{81} to An_{2}. Compositional continuity becomes more obvious in the Sr concentrations, where plagioclase analyses of gabbroic enclaves fill the gap between basaltic and trachytic melts (Fig. 14).

We conclude that no compositional gap is recorded in plagioclase phenocrysts, which represent a dominant fractionation phase in co-genetic basalt and trachyte rocks (with the exception of picritic basalt). Plagioclase fractionation was continuous during the evolution from basaltic to trachytic rocks. The chemical trends and complex disequilibrium textures in plagioclase from intermediate lavas (Fig. 14), however, suggest that erupted intermediate compositions are the product of mingling and mixing processes of mafic and silicic magmas, as pointed out by Reubi and Blundy (2009).

PETROGENIC MODEL FOR 'EARLY' AKAROA VOLCANO

On the basis of the previous two discussion chapters we propose a two-stage model for the magmatic evolution of Akaroa Volcano and the formation of a Daly Gap (Fig. 22): (1) Basaltic magmatism forms alkali basalt to hawaiites-mugearites compositions as a result of polybaric fractionation; and (2) punctuated melt extraction from an intermediate, hawaiite-mugearite crystal mush generates trachytic magmatism and a "Daly Gap".

(1) Basaltic magmatism

Crystal-rich, glomerophyyric picritic basalts likely represent erupted batches of a differentiated, primitive crystal mush. Petrologic observation and geobarometric estimates of these lavas suggest that primitive magmas crystallised and fractionated within the uppermost mantle near the crust-mantle boundary, where magmas were cooled rapidly by the overlying colder lithosphere. The base of the crust beneath Banks Peninsula has been inferred at depths of 25 to 30km (Thomson and Evison 1962, Wellman and Latter 1989, Sewell et al. 1993), which correlates with pressure estimates from clinopyroxene-liquid compositions of crystal-rich picritic basalt (9 to 11 kbar; Table 8).

Most ascending picritic basalts stagnated and fractionated at mid-crustal levels of 5 to 6 kbar (Table 8-10), which corresponds to depths of 15 to 20 km. Here, plagioclase crystallisation dominated and caused magma differentiation along a more sodic trend to form alkali basalt and hawaiite. These fractional crystallisation processes were periodically interrupted by recharge events of hotter more mafic magma, recorded as reversed zoning in plagioclase phenocrysts (Fig. 14; Streck 2008). Oscillatory zoning in plagioclase may also partially account for convective self-mixing processes (Couch et al. 2001). Magnetite and ilmenite pairs indicate recharge events and a change in the magmatic conditions (i.e. temperature) prior eruption preventing sufficient time to re-equilibrate.

(2) Trachytic magmatism

The formation of trachyte could have occurred during a period of repose in the Early Phase, where no or little magma recharge took place. Without magma replenishment, the high temperature gradients between the country rock and the magma chamber support rapid cooling along the chamber ceiling and chamber walls (Marsh 1981) leading to extensive fractionation and high viscosities. Hindered settling and compaction allowed the physical extraction of trachytic melts from a hawaiite-mugearite crystal mush (1 to 2 wt.% H_2O) within a crystal fraction of 50 to 80 vol.%.

Petrological and geochemical observation and the result from the MELTS models indicate that the Tikao Trachyte has formed via punctuated melt extraction from a hawaiite crystal mush which may be geochemically similar the erupted lavas of the older Harbour Formation. The results from the clinopyroxene P-T-estimates suggest that this process occurred near the ductile-brittle transition at about 3 kbar and 965°C (Table 8). Our field observations indicate that the Tikao Trachyte intruded after a sequence of explosive trachytic eruptions of the Lushington breccia. The geochemical trends suggest that the more evolved Lushington breccia deposits are co-genetic and therefore might have evolved in a shallow layered magma chamber by step-filling (Orsi et al. 1995). The two distinct zircon populations in trachyte (Fig. 6) might indeed reflect different trachyte melts that assembled from punctuated magma pulses from cumulative mushes below.

The results from the amphibole thermometers are consistent with amphibole crystallising at lower temperatures than pyroxene, but at fairly similar pressures. Amphibole crystallisation becomes stable at bulk-rock water contents of 3 to 5 wt.%, which indicates that amphibole-bearing trachyte are either derived from a wetter magma batch or that amphibole-bearing trachyte was extracted at a higher crystal fraction with water contents being three to four times higher than initial bulk water concentrations (i.e. at 75% crystallinity, H_2O = 4 to 8 wt.%). In addition, temperature dependent amphibole substitutions (Fig. 18) suggest that trachyte magmas got heated

prior to eruption. Hence, it is likely that recharge of hot mafic magma has triggered the trachyte eruption, a mechanism that has been widely recognised (Sparks et al. 1977, Eichelberger 1995, Murphy et al. 1998).

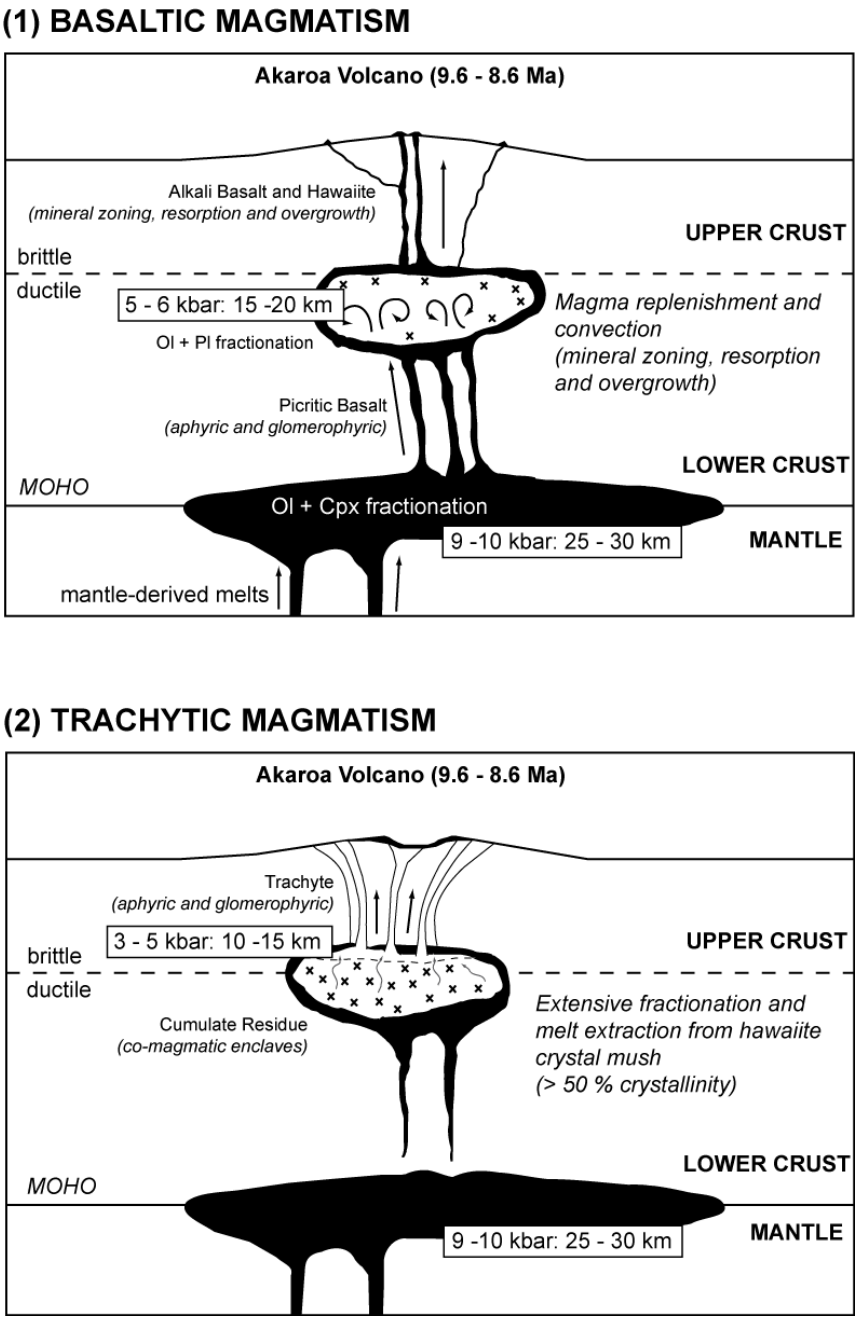

Fig. 22: Magma evolution of Akaroa Volcano occurs in a two-stage model: (1) Basaltic magmatism starts at the mantle-crust boundary with the formation of picritc basalt, which subsequently ascents to shallower levels. Olivine and plagioclase fractionation produce alkali basalt and hawaiite compositions. Frequent magma replenishment and vigorous convection leads to complex mineral zoning and eruption of mafic lavas; (2) Extensive fractionation of hawaiite magmas lead to the formation of a crystal rich mush. Once the crystallinity has reached more than 50 vol.% crystals, melt can be extraction to form trachytic melts that erupt at the surface.

CONCLUDING REMARKS

The geochemical and petrological results of this study lead to the following conclusion regarding the magmatic evolution and formation of a “Daly Gap” at Akaroa Volcano.

(1) The alkali trends from picritic basalt to trachyte at Akaroa Volcano can be related by crystal fractionation processes in a two-stage model, which has been quantitatively tested (e.g MELTS). The first stage produces alkali basalt and hawaiite from a picritic source. The second stage produces trachyte and a Daly Gap from melt extraction within an optimal window of 50 to 80 vol.%.

(2) Basaltic magmatism started at the mantle-crust boundary, where picritc basalt separated from a primitive olivine-clinopyroxene dominated crystal mush. Ascending magmas stalled at mid-crustal levels (15 to 20 km) and fractionate a low-pressure assemblage (olivine + plagioclase) that produced the observed alkali basalt and hawaiite compositions

(3) Episodically magma replenishment of hotter more mafic caused local mingling and mixing and vigorous convection within the shallow magma chamber reservoir recorded in the reversed zoned plagioclase phenocrysts.

(4) Periods of repose could have initiated the differentiation towards trachytic melts. Trachytic liquids were physically separated from a hawaiite-mugearite crystal mush stored at 10 to 15 km near the brittle ductile transition. The restriction of melt extraction within an optimal window of 50 to 80 vol% has also caused the observed bimodal distribution (Daly Gap) of erupted lavas.

(5) Co-genetic magmatic enclaves are likely to represent crystal cumulates and support trachyte formation by melt extraction (e.g. trace element models, mineral records).

This study contributes to the recent understanding of the magmatic evolution of Akaroa Volcano. The presented model can explain the origin of trachyte and the bimodal nature of erupted

lavas in the Early Phase. However, additional research is needed on the late phase trachytes and the plutonic rocks on Onawe Peninsula to apply this model to the whole volcano. Furthermore, new age constraints on the Early Phase deposits could be helpful to establish time constraints on the physical liquid-crystal separation processes (i.e. hindered settling vs. compaction modelling) and to answer the question whether the Tikao Trachyte or the Lushington Breccia represent the older eruption.

REFERENCES

Abbott MJ 1969. Petrology of the Nandewar Volcano, N.S.W., Australia. Contributions to Mineralogy and Petrology 20: 115-134

Anderson JL 1996. Status of thermobarometry in granitic batholiths. Transactions of the Royal Society of Edinburgh: Earth Sciences 87: 125-138

Anderson JL, Smith DR 1995. The effects of temperature and $fO2$ Al-in-hornblende barometer. American Mineralogist 80: 549-559

Bachmann O, Bergantz GW 2004. On the Origin of Crystal-poor Rhyolites: Extracted from Batholithic Crystal Mushes. Journal of Petrology 45: 1565-1582

Bachmann O, Bergantz GW 2008. Rhyolites and their Source Mushes across Tectonic Settings. Journal of Petrology 49: 2277-2285

Bachmann O, Dungan M.A 2002. Temperature-induced Al-zoning in hornblendes of the Fish Canyon magma, Colorado. American Mineralogist 87: 1062-1076

Baker I 1968. Intermediate Oceanic Volcanic Rocks and the 'Daly Gap'. Earth and Planetary Science Letters 4: 103-106

Barley ME, Weaver SD, de Laeter JR 1988. Strontium isotope composition and geochronology of intermediate-silicic volcanics, Mt Somers and Banks Peninsula, New Zealand. New Zealand Journal of Geology and Geophysics 31: 197-206

Barth TFW, Correns CW, Eskola P 1939. Die Entstehung der Gesteine, Springer-Verlag, Berlin. 442p.

Best MG 2003. Igneous and Metamorphic Petrology, Blackwell Science Ltd.. Oxford. 729p

Bonin B 2007. A-type granites and related rocks: Evolution of a concept, problems and prospects. Lithos 97: 1-29

Blundy JD, Holland TJB 1990. Calcic amphibole equilibria and a new amphibole-plagioclase geothermometer. Contributions to Mineralogy and Pe-trology 104: 208–224

Bonnefoi CC, Provost A, Albarede F 1995. The "Daly gap" as a magmatic catastrophe. Nature 378: 270-272

Bowen NL 1928. The Evolution of Igneous Rocks. Princeton University Press, Princeton. 334 p.

Brophy JG 1991. Composition gaps, critical crystallinity, and fractional crystallization in orogenic (calc-alkaline) magmatic systems. Contributions to Mineralogy and Petrology 109: 173-182

Bunsen R (1851). Ueber die Prozesse der vulkanischen Gesteinsbildungen Islands: Annalen der Physik 83: 197-272

Chayes F 1963. Relative Abundance of Intermediate Members of the Oceanic Basalt-Trachyte Association. Journal of Geophysical Research 68: 1519-1534

Chayes F 1977. The oceanic basalt-trachyte relation in general and in the Canary Islands. American Mineralogist 62: 666-671

Clague DA 1978. The Oceanic Basalt-Trachyte Association: An Explanation of the Daly Gap. Journal of Geology 86: 739-743

Couch S, Sparks RSJ, Carroll MR 2001. Mineral disequilibrium in lavas explained by convective self-ixing in open magma chambers. Nature 411: 1037-1039

Daly RA 1925. The geology of Ascension Island. American Academy of Arts and Sciences Proceedings 60: 1-80

Deering CD 2009. Cannibalization of an amphibole-rich andesitic progenitor induced by caldera-collapse during the Matahina eruption: Evidence from amphibole compositions. American Mineralogist 94: 1162-1174

Deering CD, Bachmann O, Dufek J, Gravley D (in review). Rift-Related Transition From Andesite to Rhyolite Volcanism in the Taupo Volcanic Zone (New Zealand) Controlled by Crystal-Melt Dynamics in Mush Zones With Variable Mineral Assemblages. Journal of Petrology

Deering CD, Bachmann O 2010. Trace element indicators of crystal accumulation in silicic igneous rocks. Earth and Planetary Science Letters 297: 324-331

Dorsey CJ 1988: The geology and geochemistry of the Akaroa volcano, Banks Peninsula, New Zealand. Unpublished PhD thesis, University of Canterbury, Christchurch, New Zealand.

Dufek J, Bergantz GW 2005. Lower Crustal Magma Genesis and Preservation: a Stochastic Framework for the Evaluation of Basalt-Crust Interaction. Journal of Petrology 46: 2167-2195

Dufek J, Bachmann O 2010. Quantum magmatism: Magmatic compositional gaps generated by melt-crystal dynamics. Geology 38: 687-690

Eichelberger JC 1995. Silicic volcanism: ascent of viscous magmas from crustal reservoirs. Annual Review of Earth and Planetary Science Letters 23: 41-63

Eichelberger JC, Izbekov PE, Browne BL 2006. Bulk chemical trends at arc volcanoes are not liquid lines of descent. Lithos 87: 135-154

Ernst WG, Liu J 1998. Experimental phase-equilibrium study of Al- and Ti- contents of calcic amphibole in MORB-A semiquantitative thermobarometer. American Mineralogist 83: 952-969

Falloon TJ 1982. The geology of the Onawe - French Farm - Wainui area, Akaroa volcano, Banks Peninsula. Unpublished BSc Hons thesis, University of Canterbury, Christchurch, New Zealand.

Féménias O, Mercier JCC, Nkono C, Diot H, Berza T, Tatu M, Demaiffe D 2006. Calcic amphibole growth and compositions in calc-alka- line magmas: Evidence from the Motru Dike Swarm (Southern Carpathians, Romania). American Mineralogist 91: 73-81

Ferla P, Meli C 2006. Evidence of Magma Mixing in the “Daly Gap” of Alkaline Suites: a Case Study from the Enclaves of Pantelleria (Italy). Journal of Petrology 47: 1467-1507

Fowler SJ, Spera FJ 2010. A Metamodel for Crustal Magmatism: Phase Equilibria of Giant Ignimbrites. Journal of Petrology 51: 1783-1830.

France L, Ildefonse B, Koepke J, Bech F 2010. A new method to estimate the oxidation state of basaltic series from microprobe analyses. Journal of Volcanology and Geothermal Research 189: 340-346

Ghiorso MS, Sack RO 1995. Chemical Mass Transfer in Magmatic Processes. IV. A Revised and Internally Consistent Thermodynamic Model for the Interpolation and Extrapolation of Liquid-Solid Equilibria in Magmatic Systems at Elevated Temperatures and Pressures. Contributions to Mineralogy and Petrology 119: 197-212

Ghiorso MS, Hirschmann MM, Reiners PW, Kress VC III 2002. The pMELTS: An revision of MELTS aimed at improving calculation of phase relations and major element partitioning involved in partial melting of the mantle at pressures up to 3 GPa. Geochemistry, Geophysics, Geosystems 3(5), 10.1029/2001GC000217

Hammarstrom JM, Zen E 1986. Aluminum in hornblende: An empirical igneous geobarometer. American Mineralogist 71: 1297-1313

Hampton SJ, Cole JW 2009. Lyttelton Volcano, Banks Peninsula, New Zealand: Primary volcanic landforms and eruptive centre identification. Geomorphology 104: 284-298

Harris PG 1963. Comments on a paper by F. Chayes, "Relative abundance of intermediate members of the oceanic basalt-trachyte association": Journal of Geophysical Research 68: 5103-5107

Hess PC (1992). Phase equilibria constraints on the origin of ocean floor basalts. In: Phipps Morgan J , Blackman DK, Sinton JM (eds) Mantle Flow and Melt Generation at Mid-Ocean Ridges. American Geophysical Union, 67-102

Hildreth W 2004. Volcanological perspectives on Long Valley, Mammoth Mountain, and Mono Craters: several contiguous but discrete systems. Journal of Volcanology and Geothermal Research 136: 169-198

Holland T, Blundy J 1994. Non-ideal interactions in calcic amphiboles and their bearing on amphibole-plagioclase thermometry. Contributions to Mineralogy and Petrology 116: 433-447

Hollister LS, Grissom GC, Peters EK, Stowell HH, Sisson VB 1987. Confirmation of the empirical correlation of Al hornblende with pressure of solidification of calc-alkaline plutons. American Mineralogist 72: 231-239

Johnson, M.C. and Rutherford, M.J., 1989a. Experimentally determined conditions in the Fish Canyon Tuff, Colorado, magma chamber. Journal of Petrology, 30, pp.711–737

Johnston DM, Cole JW, Houghton BF 1997. Physical volcanology of Miocene basaltic pyroclastic deposits at Pigeon Bay: remnants of flank scoria cones of Akaroa volcano, Banks Peninsula, New Zealand. New Zealand Journal of Geology and Geophysics 40: 109-115

Leake BE, Wooley AR, Arps CES, Birch WD, Gilbert MC, Grice JD, Hawthrone FC, Kato A, Kisch HJ, Krivovichev VG, Linthout K, Laird J, Mandarino JA, Maresch WV, Nickel EH, Rock NMS, Schumacher JC, Smith DC, Stephensen NCN, Ungaretti L, Whittaker EJW, Youzhi G 1997. Nomenclature of amphiboles: Report of the Subcommittee on Amphiboles of the International mineralogical Association, Commission on New Minerals and Mineral Names. American Mineralogist 82: 1019-1037

Le Maitre RW, Streckeisen A, Zanettin B, Le Bas MJ, Bonin B, Bateman P, Bellieni G, Dudek A, Efremova S, Keller J, Lamere J, Sabine PA, Schmid R, Sorensen H, Woolley AR 2002. Igneous Rocks: A Classification and Glossary of Terms, Recommendations of the International Union of Geological Sciences, Subcommission of the Systematics of Igneous Rocks. Cambridge University Press

Liggett KA, Gregg DR 1965. Geology of Banks Peninsula. In: Thompson BN, Kermode LO eds. New Zealand Volcanology, South Island. New Zealand Geological Survey Information Series 51: 9-25

Macdonald GA 1963. Relative abundance of intermediate members of the oceanic basalt- trachyte association - a discussion. Journal of Geophysical Research 68: 5100-5102

Marsh BD 1981. On the crystallinity, probability of occurrence, and rheology of lava and magma. Contributions to Mineralogy and Petrology 78: 85-98

Murphy MD, Sparks RSJ, Barclay J, Carroll MR, Lejeune AM, Brewer TS, Macdonald R, Black S and Young S 1998. The role of magma mixing in triggering the current eruption at the Soufriere Hills volcano, Montserrat, West Indies. Geophysical Research Letters 25: 3433-3436

Nekvasil H 2004. The Origin and Evolution of Silica-saturated Alkalic Suites: an Experimental Study. Journal of Petrology 45: 693-721

Nimis P 1995. A clinopyroxene geobarometer for basaltic systems based on crystals-structure modeling. Contributions to Mineralogy and Petrology 121: 115-125

Nimis P, Taylor WR 2000. Single clinopyroxene thermobarometry for garnet peridotites. Part 1 Calibration and testing of a Cr-in-cpx barometer and an enstatite-in-cpx thermometer. Contributions to Mineralogy and Petrology 139: 541-554

Nimis P, Ulmer P 1998. Clinopyroxene geobarometry of magmatic rocks. Part 1: an expanded structural geobarometer for anhydrous and hydrous basic and ultrabasic systems. Contributions to Mineralogy and Petrology 133: 122-135

O'Hara MJ 1965. Primary magmas and the origin of basalts. Scottish Journal of Geology 1: 19-40

Orsi G, Civetta L, Antonio MD, Di Girolamo P, Piochi M 1995. Step-filling and development of a three-layer magma chamber: the Neapolitan Yellow Tuff case history. Journal of Volcanology and Geothermal Research 67: 291-312

Petford N, Gallagher K 2001. Partial melting of mafic (amphibolite) lower crust by periodic influx of basaltic magmas. Earth and Planetary Science Letters 193: 483-499

Price RC, Chappell BW 1975. Fractional Crystallization and the petrology of Dunedin Volcano. Contributions to Mineralogy and Petrology 53: 157-182

Price RC, Taylor SR 1980. Petrology and geochemistry of the Banks Peninsula volcanoes, South Island, New Zealand. Contributions to Mineralogy and Petrology 72: 1-18

Putirka K, Johnson M, Kinzler R, Longhi J, Walker D 1996. Thermobarometry of mafic igneous rocks based on clinopyroxene-liquid equilibria, 0-30 kbar. Contributions to Mineralogy and Petrology 123: 92-108

Putirka K, Ryerson FJ, Mikaelian H 2003. New igneous thermobarometers for mafic and evolved lava compositions, based on clinopyroxene + liquid equilibria. American Mineralogist 88: 1542-1554

Putirka K 2008. Thermometers and Barometers for Volcanic Systems. Reviews in Mineralogy and Geochemistry 69: 61-120

Reubi O, Blundy J 2009. A dearth of intermediate melts at subduction zone volcanoes and the petrogenesis of arc andesites. Nature 461: 1269-1273

Rice A 1981. Convective fractionation: A mechanism to provide cryptic zoning (macrosegregation), layering, crescumulates, banded tuffs and explosive volcanism in igneous processes. Journal of Geophysical Research 86: 405-417

Ridolfi F, Renzulli A, Puerini M 2009. Stability and chemical equilibrium of amphibole in calc-alkaline magmas: an overview, new thermobarometric formulations and application to subduction-related volcanoes. Contributions to Mineralogy and Petrology 160: 45-66

Roedder PL, Emslie RF 1970. Olivine-liquid equilibrium. Contributions to Mineralogy and Petrology 29: 275-289

Scaillet B, Evans BW 1999. The 15 June 1991 eruption of Mount Pinatubo. I. Phase equilibria and pre-eruption P-T-fO2-fH2O conditions of the dacite magma. Journal of Petrology 40: 381-411

Schmidt MW 1992. Amphibole composition in tonalite as a function of pressure; an experimental calibration of the Al-in-hornblende barometer. Contributions to Mineralogy and Petrology 110: 304-310

Sewell RJ 1985. The volcanic geology and geochemistry of central Banks Peninsula and relationships to Lyttelton and Akaroa volcanoes. Unpublished PhD thesis, University of Canterbury, Christchurch, New Zealand.

Sewell RJ 1988. Late Miocene volcanic stratigraphy of central Banks Peninsula, Canterbury, New Zealand. New Zealand Journal of Geology and Geophysics 31: 41-64

Sewell RJ, Hobden BJ, Weaver SD 1993. Mafic and ultramafic mantle and deep crustal xenoliths from Banks Peninsula, South Island, New Zealand. New Zealand Journal of Geology and Geophysics 36: 223-231

Sparks RSJ, Sigurdsson H, Wilson L 1977. Magma mixing: a mechanism for triggering acid explosive eruptions. Nature 267: 315-318

Sparks RSJ, Huppert HE, Turner JS, Sakuyama M, O'Hara MJ 1984. The Fluid Dynamics of Evolving Magma Chambers [and Discussion]. Philosophical Transactions of the Royal Society. Series A, Mathematical and Physical Sciences 310: 511-534

Spear FS 1981. An experimental study of hornblende stability and compositional variability in amphibolite. American Journal of Science 281: 697-734

Speight R 1917: The geology of Banks Peninsula. Transactions of the Royal Society of New Zealand 49: 365-392

Speight R 1923. The intrusive rocks of Banks Peninsula. Records of the Canterbury Museum 2: 121-150

Speights R 1940. The basal beds of the Akaroa Volcano. Transactions of the Royal Society of New Zealand 70: 60-76

Speight R 1944. The geology of Banks Peninsula: a revision, Part II, the Akaroa Volcano. Trans. R. Soc. N.Z. 74: 232-54

Stipp JJ, McDougall I 1968. Geochronology of the Banks Peninsula Volcanoes. New Zealand Journal of Geology and Geophysics 11: 1239-1260

Streck MJ 2008. Mineral Textures and Zoning as Evidence for Open System Processes. Reviews in Mineralogy and Geochemistry 69: 595-622

Thiele B 1983. Basement geology of the Lyttelton Volcano, Banks Peninsula. Unpublished MSc thesis, University of Canterbury, Christchurch, New Zealand.

Thomas WM, Ernst WG 1990. The aluminum content of hornblende in calc-alkaline granitic rocks: A mineralogic barometer calibrated experimentally to 12 kbars. In: Spencer RJ, Chou IM eds. Fluid-Mineral Interactions: A Tribute to H.P. Eugster. Geochemical Society Special Publication 2: 59-63

Thompson RN 1972. Evidence for a chemical discontinuity near the basalt-andesite transition in many anorogenic volcanic suites: Nature 236: 106-110

Thomson AA, Evison FF 1962. Thickness of the earth's crust in New Zealand. New Zealand Journal of Geology and Geophysics 5: 29-45

Timm C, Hoernle K, Van Den Bogaard P, Bindeman I, Weaver S 2009. Geochemical Evolution of Intraplate Volcanism at Banks Peninsula, New Zealand: Interaction Between Asthenospheric and Lithospheric Melts. Journal of Petrology 50: 989-1023

Van Haast J 1860. Report of a geological survey of Mt Pleasant. Provincial Council of Canterbury Session XVII, December 19.

Vigneresse JL, Barbey P, Cuney M 1996. Rheological Transitions During Partial Melting and Crystallization with Application to Felsic Magma Segregation and Transfer. Journal of Petrology 37: 1579-1600

Weaver SD, Sewell RJ 1986. Cenozoic volcanic geology of the Banks Peninsula. South Island igneous rocks. In: Houghton BF, Weaver SD eds. New Zealand Geological Survey Record 13: 39-63

Weaver SD, Smith IEM 1989. New Zealand intraplate volcanism. In: Johnson RW ed. Intraplate Volcanism in Eastern Australia and New Zealand. Cambridge, Cambridge University Press: 157-188

Wellman P, Latter JH 1989. Upper mantle and crust of New Zealand. In: Johnson RW ed. Intraplate Volcanism in Eastern Australia and New Zealand. Cambridge, Cambridge University Press: 38-40

Whitaker ML, Nekvasil H, Lindsley DH, Difrancesco NJ 2006. The Role of Pressure in Producing Compositional Diversity in Intraplate Basaltic Magmas. Journal of Petrology 48: 365-393

Yoder HS, Tilley CE 1962. Origin of basaltic magmas: An experimental study of natural and synthetic systems. Journal of Petrology 3: 342-532